

26
27
28
29
30
31
32
33
34
35
36
37
38
39
40
41
42
43
44
45
46
47
48

Abstract

A new-generation meteor radar was installed at the Brazilian Antarctic Comandante Ferraz Base (62.1°S) in March 2010. This paper describes the motivations for the radar location, its measurement capabilities, and comparisons of measured mean winds, tides, and gravity wave momentum fluxes from April to June of 2010 and 2011 with those by a similar radar on Tierra del Fuego (53.8°S). Motivations for the radars include the “hotspot” of small-scale gravity wave activity extending from the troposphere into the mesosphere and lower thermosphere (MLT) centered over the Drake Passage, the maximum of the semidiurnal tide at these latitudes, and the lack of other MLT wind measurements in this latitude band.

Mean winds are seen to be strongly modulated at planetary wave and longer periods and to exhibit strong coherence over the two radars at shorter time scales as well as systematic seasonal variations. The semidiurnal tide contribute most to the large-scale winds over both radars, with maximum tidal amplitudes during May and maxima at the highest altitudes varying from ~20 to >70 ms⁻¹. In contrast, the diurnal tide and various planetary waves achieve maximum winds of ~10 to 20 ms⁻¹.

Monthly-mean gravity wave momentum fluxes appear to reflect the occurrence of significant sources at lower altitudes, with relatively small zonal fluxes over both radars, but with significant, and opposite, meridional momentum fluxes below ~85 km. These suggest gravity waves propagating away from the Drake Passage at both sites, and may indicate an important source region accounting in part for this “hotspot”.

49 1 Introduction

50 It is now well known that the structure and variability of the mesosphere and lower
51 thermosphere (MLT) is determined to a significant degree by large- and small-scale waves
52 propagating into this region from below. Tides, planetary waves (PWs), and gravity waves
53 (GWs) exhibit significant variability with season and latitude due to seasonal variations in their
54 sources and propagation environments [*e.g.*, *Holton*, 1984; *Burrage et al.*, 1995; *Vincent et al.*,
55 1998; *Manson et al.*, 1999; *Pancheva et al.*, 2002, 2004, 2009; *McLandress*, 2002; *Fritts and*
56 *Alexander*, 2003; *Lieberman et al.*, 2004; *Murphy et al.*, 2006]. GWs and tides also exhibit
57 longitudinal variability reflecting the longitudinal distributions of their forcing dynamics [*e.g.*,
58 *Tsuda et al.*, 2000; *Hagan and Forbes*, 2002, 2003; *Espy et al.*, 2006]. Indeed, there are preferred
59 latitudes and longitudes where these various motions systematically achieve their largest
60 responses. Possibly the most dramatic responses, and potential for interactions among large- and
61 small-scale motions, occur in late fall and winter at middle to high latitudes. Semidiurnal tide
62 and PW winds maximize here [*Forbes*, 1995; *Hagan and Forbes*, 2003], and GWs exhibit strong
63 responses at lower altitudes over specific source regions [*McLandress et al.*, 2000; *Ern et al.*,
64 2004; *Wu*, 2004; *Jiang et al.*, 2006; *Alexander et al.*, 2008a; *Wu and Eckermann*, 2008] that
65 clearly extend into the MLT in some cases. Most of these apparent GW source regions in both
66 hemispheres correlate with high terrain. Of these, the region encompassing the Andes, the Drake
67 Passage, and the Antarctic Peninsula appears to exhibit the largest responses on Earth [*Jiang et*
68 *al.*, 2002; *Preusse et al.*, 2002, 2006; *Wu and Jiang*, 2002; *Eckermann et al.*, 2006; *Wu et al.*,
69 2006; *Alexander et al.*, 2008b; *Hertzog et al.*, 2008]. Indeed, this region has yielded a number of
70 examples of strong interactions among these various motions, despite limited observational
71 capabilities until recently [*Smith et al.*, 2009; *Beldon and Mitchell*, 2010; *Fritts et al.*, 2010a, b].

72 The large amplitudes anticipated for the various tidal, PW, and GW motions in the Drake
73 Passage “hotspot”, and our expectation for strong interactions among these various motions,
74 were the motivations for placing two new-generation meteor radars in the northern and southern
75 portions of this natural laboratory for MLT dynamics studies. The Southern Argentina Agile
76 MEteor Radar (SAAMER) was installed at Rio Grande on Tierra del Fuego (53.8°S, 67.8°W) in
77 May 2008, and a nearly identical system, the Drake Antarctic Agile MEteor Radar (DrAAMER),
78 was installed at the Brazilian Antarctic Comandante Ferraz Base (62.1°S, 58.7°W) in March
79 2010. The two radars were specifically designed to measure both the large-scale (mean, tidal,
80 and PW) motion fields with high precision and the vertical fluxes of horizontal momentum by
81 GWs, the latter of which previously has only been possible with significantly larger and more
82 expensive radars and lidars. SAAMER capabilities for mean, tidal, and PW wind measurements
83 were demonstrated by *Fritts et al.* [2010a, 2011a, hereafter *F10a* and *F11a*]. The potential for
84 GW momentum flux measurements was evaluated and first employed using SAAMER by *Fritts*
85 *et al.* [2010b, hereafter *F10b*].

86 An additional capability that we hope will be demonstrated with these radars with further
87 analysis is the potential to measure GW-tidal and GW-PW interactions and their modulation of
88 GW variances and momentum fluxes. Such interactions have been observed in limited MLT
89 observations [*Fritts and Vincent*, 1987; *Wang and Fritts*, 1991; *Thayaparan et al.*, 1995; *Isler*
90 *and Fritts*, 1996; *Manson et al.*, 1998; *Murphy and Vincent*, 1998; *Preusse et al.*, 2001; *Espy et*
91 *al.*, 2004; *Beldon and Mitchell*, 2010] and in numerical models of these dynamics [*Holton*, 1984;
92 *Miyahara* 1985; *Miyahara et al.*, 1986; *Forbes et al.*, 1991; *Lu and Fritts*, 1993; *Eckermann and*
93 *Marks*, 1996; *Meyer*, 1999; *Ortland and Alexander*, 2006; *Liu et al.*, 2008]. They have yet to be
94 fully quantified, understood, and adequately parameterized in large-scale models, however

95 [McLandress and Ward, 1994; McLandress, 1998, 2002; Hagan *et al.*, 1999; Fritts and
96 Alexander, 2003], hence such measurements where these interaction dynamics are particularly
97 strong would prove valuable in constraining such efforts.

98 Our purposes in this paper are to describe the DrAAMER radar system and compare its
99 measurement capabilities for large- and small-scale MLT dynamics with those of SAAMER for
100 April, May, and June of its first two years of operation. The radar configuration, the spatial and
101 temporal variations of meteor detections observed from Ferraz, and our data analysis methods
102 are described in Section 2. DrAAMER mean and tidal winds during April, May, and June of
103 2010 and 2011 are described and compared with those measured by SAAMER from 2009 to
104 2011 and with the Global-Scale Wave Model, version 2009 [GSWM-09, see Zhang *et al.*, 2010a,
105 b] in Sections 3 and 4. Section 5 compares monthly-mean GW momentum fluxes estimated by
106 DrAAMER and SAAMER during April, May, and June 2010 and 2011. A discussion of these
107 results and our summary and conclusions are provided in Sections 6 and 7. A separate
108 assessment by Fritts *et al.* [2011b] of DrAAMER GW momentum flux measurement capabilities
109 compared to SAAMER and three other meteor radars explores the potential for similar
110 measurements with traditional meteor radars.

111 **2 DrAAMER System Description and Data Analysis**

112 **a. System description**

113 Like SAAMER [F10a, F10b], DrAAMER was specifically configured to enable high-
114 resolution definition of the large-scale wind field and potential sensitivity to GW momentum
115 fluxes employing a generalization of the dual-beam technique first employed by Vincent and
116 Reid [1983] and extended to multiple-beam studies by VanZandt *et al.* [1990] and Fritts *et al.*
117 [1990]. Definition of both the large-scale motion field at high resolution and GW momentum

118 fluxes requires high meteor count rates at sufficiently small off-zenith angles to allow vertical
119 motions due to GWs to make significant contributions to the inferred radial velocities. As with
120 SAAMER, this was accomplished through significantly higher peak power than employed by
121 typical meteor radars and a transmitting array that directs the majority of radar power into eight
122 beams at 45° azimuth increments with peak power at ~35° off zenith. This results in a majority of
123 meteor detections at off-zenith angles between 15 and 50°. The SAAMER and DrAAMER
124 antenna patterns, daily counts, and altitude distributions of accepted meteors are illustrated for
125 one day in the upper panel and for April, May, and June 2011 in the lower panels of Figure 1.
126 All-sky unambiguous meteor detections achieving a threshold accuracy (~50% of the totals)
127 average ~19,800 and ~8,500 per day at SAAMER and DrAAMER, respectively.

128 DrAAMER radar parameters and measurement capabilities include:

- 129 1) a radar frequency of 36.9 MHz and bandwidths ranging from 35 to 125 kHz,
- 130 2) a peak transmitter power of 30 kW,
- 131 3) a transmitter antenna composed of eight three-element crossed Yagis in a circle of
132 diameter 24.4 m having opposite phasing of every other Yagi (normal mode),
- 133 4) five receiver channels to reduce meteor position ambiguities [*Jones et al.*, 1998],
- 134 5) a transmit/receive (T/R) switch allowing both tropospheric measurements and use of the
135 transmitter antenna as a sixth receiver,
- 136 6) a transmitter phasing option that allows power to be directed vertically,
- 137 7) various pulse-coding, pulse repetition frequency (PRF), and integration options, and

138 8) sufficient power and beam definition flexibility to perform enhanced meteoroid radiant,
139 population size, and “head echo” studies normally possible only with high-power, large-
140 aperture (HPLA) radars.

141 Since commissioning, DrAAMER has employed a 2-bit code, a PRF of 1730 Hz, integration
142 over four samples, and meteor sampling at altitudes from 70 to 110 km.

143 **b. Date analysis**

144 Mean and tidal winds are obtained from hourly-mean zonal and meridional winds in 3-
145 km altitude bins from ~78 to 99 km employing radial velocities at off-zenith angles between 15
146 and 50°. These estimates include ~50 and 100 meteors/hr near 90 km on average over
147 DrAAMER and SAAMER, respectively, and a minimum of 5 meteors/hr is required for a valid
148 horizontal wind estimate at the higher and lower altitudes. Daily-mean zonal and meridional
149 winds and diurnal and semidiurnal tide amplitudes are determined employing a continuous “S-
150 transform” [Stockwell *et al.*, 1996] Gaussian wavelet analysis applied to the hourly-mean winds.
151 Monthly-mean winds and tidal amplitudes are computed for 2010 and 2011 from daily means for
152 which a minimum of 12 hourly-mean wind estimates are available, with missing daily means
153 interpolated from 3rd-order spline fits. We present daily-mean winds and tides over DrAAMER
154 only for 2011, however, due to five ~3 to 10-day intervals during May and June 2010 for which
155 no data were obtained. Zonal and meridional wind spectra spanning the 3-month analysis period
156 during 2011 are computed from the hourly-mean winds at 90 km.

157 Monthly GW momentum fluxes are estimated using the method of *Hocking* [2005]
158 following removal of mean and tidal winds derived from “S-transform” fits to the hourly-mean
159 winds. S-transform means and tidal amplitudes employed for these assessments allow more
160 complete removal of varying mean and tidal motions in the presence of data gaps, as seen in the

161 DrAAMER data in Figure 1. A three-point triangular smoothing is used to reduce estimation
162 uncertainties. Such monthly momentum flux assessments were evaluated extensively by *F10b*
163 and found to yield reasonable estimates for a wide range of test fields employing SAAMER.

164 **3 Mean Winds and Spectra**

165 We present here daily-mean and monthly-mean winds, and their S-transforms, over
166 DrAAMER and SAAMER to illustrate their similarities and differences on daily-to-inter-annual
167 time scales. Daily-mean winds over SAAMER are displayed for April, May, and June of 2009,
168 2010, and 2011 (top to bottom) in Figure 2. Daily-mean winds over DrAAMER for April, May,
169 and June 2011 are shown in the upper panels of Figure 3. Corresponding S-transforms of the
170 daily-mean winds over SAAMER for the three years are shown in the upper and lower left three
171 panels of Figure 4, with those over DrAAMER for 2011 shown in the right panels. Monthly-
172 mean winds over the two radars for April, May, and June (top to bottom) of 2010 and 2011 are
173 shown in Figure 5. Zonal and meridional wind and tidal amplitude components are shown at left
174 and right, respectively, in Figures 2, 3, and 5, and at top and bottom in Figure 4. Spectra of the
175 hourly-mean zonal and meridional winds during April to June 2011 over DrAAMER centered at
176 88.5 km are shown for periods from 2 hr to ~40 days in the upper and lower panels of Figure 6,
177 respectively.

178 Daily-mean winds over SAAMER during 2009, 2010, and 2011 reveal similar seasonal
179 trends each year, with weak westward or eastward mean winds during April and increasingly
180 eastward mean winds arising during May and June at all altitudes. Westward maxima approach
181 $\sim 20 \text{ ms}^{-1}$ in April, while eastward maxima reaching $\sim 50 \text{ ms}^{-1}$ become much more prevalent in
182 May and June of each year. Meridional wind maxima vary from ~ -30 to 30 ms^{-1} throughout
183 these three months each year. PWs and longer-period oscillations ranging from periods of ~ 2 to

184 40 days or longer are seen to occur each year and to contribute to the maximum zonal and
185 meridional winds throughout each interval. As described by *F11a*, the PWs observed over
186 SAAMER having periods from ~8 to 20 days exhibit significant temporal variability and a range
187 of phase relationships among the wind components, suggesting strong transience and interactions
188 among the various PW and tidal motions. In particular, inspection of Figure 2 indicates that the
189 broader eastward wind maxima appear to correlate most strongly with southward meridional
190 winds each year (see the eastward maxima centered in mid May 2009, mid-to-late May and early
191 and late June of 2010, and mid May and late June 2011). Mean winds over DrAAMER during
192 2011 (Figure 3, top) closely resemble those over SAAMER throughout these three months,
193 indicating that the spatial scales of the mean winds and the PW and longer-period oscillations are
194 significantly greater than the separation between the two radars.

195 Longer-period oscillations were not addressed by *F11a*, but were seen to occur in the S-
196 transforms of the mean winds in Figure 3 of that study. S-transforms of the mean winds
197 displayed in Figure 4 exhibit the relative contributions of PWs and longer-period oscillations to
198 the zonal and meridional winds throughout each season over SAAMER and for 2011 over
199 DrAAMER. Over SAAMER, significant modulations of the mean winds occur at periods from
200 ~5 to 40 days, with the most prevalent oscillations of ~5 to 10-day periods throughout 2009 and
201 2010 and primarily during June of 2011, ~15 to 20-day periods from April into May 2009, from
202 late April into June 2010, and during May and June 2011, and ~30 to 45-day periods contributing
203 throughout 2009 and primarily during June of 2010 and 2011, respectively. SAAMER and
204 DrAAMER mean wind S-transforms for 2011 exhibit some similarities, but also clear
205 differences, at ~5 to 15-day periods throughout, with very strong correlations in their temporal
206 variability largely in late May and June at periods of ~20 days and longer.

207 Monthly-mean zonal and meridional winds over DrAAMER and SAAMER (red and
208 blue, respectively) are compared for 2010 and 2011 (solid and dashed, respectively) in Figure 5.
209 Monthly-mean zonal winds in April are weak and eastward in all cases ($\sim 10 \text{ ms}^{-1}$ or less), despite
210 the sporadic negative excursions seen to accompany PW and longer-period oscillations in
211 Figures 2 and 3. Mean zonal winds increase by ~ 5 to 10 ms^{-1} from April to May, with somewhat
212 larger increases in 2010 and over SAAMER compared to DrAAMER. Mean zonal winds
213 increase again by ~ 5 to 10 ms^{-1} from May to June over SAAMER, with the larger increases at
214 middle and higher altitudes. DrAAMER mean zonal winds, however, increase very little from
215 May to June, with the largest changes below $\sim 90 \text{ km}$ in 2011.

216 Monthly-mean meridional winds during both 2010 and 2011 in all three months remain
217 between ~ -5 and 5 ms^{-1} , except over SAAMER, and over DrAAMER in May 2011, at the higher
218 altitudes. Note that monthly-mean winds are not displayed over DrAAMER above 96 km for
219 several months due to a lack of sufficient meteor detections to satisfy our measurement
220 constraints. While mean meridional winds over both radars during June 2010 below $\sim 90 \text{ km}$ are
221 equatorward rather than poleward (as expected to result from GW driving of the residual
222 circulation and implying subsidence in the winter polar mesosphere), there are several factors
223 that may account for this behavior. As noted by *F10b*, the winter jet in June over SAAMER
224 typically extends to higher altitudes, with a weaker (poleward, as seen) residual circulation at
225 even higher altitudes, than seen at other sites. This response may be linked to unusual GW
226 forcing of the MLT over the Drake Passage “hotspot” [see *F10b*] that will be discussed further
227 below. There is also considerable variability imposed by PWs and longer-period oscillations that
228 may influence estimates of monthly-mean meridional motions at the level of the variations seen
229 to occur in Figure 5.

230 Spectra of hourly-mean zonal and meridional velocities centered at 88.5 km over
231 DrAAMER spanning periods from 2 hr to ~40 days are shown in the upper and lower panels of
232 Figure 6, respectively. These spectra closely resemble those obtained over SAAMER by *F10a*,
233 with maximum power in the semidiurnal tide, a clear but weaker diurnal peak, and distinct
234 terdiurnal peaks. Also seen is an apparent continuum of GW motions at periods shorter than the
235 inertial period at the DrAAMER latitude (~13.6 hr), a sharper apparent decrease in spectral
236 power near the inertial period than seen over SAAMER, and evidence of PW variance
237 enhancements at longer periods than the diurnal tide, with comparable variances in the zonal and
238 meridional components at periods from ~1 to 10 days and somewhat larger zonal variances at
239 longer periods. We note also that GW variances are likely greater than implied by these spectra
240 because the hourly fits to the meteor winds from which the spectra were computed do not capture
241 GW structures having significant horizontal phase variations across the central radar beams
242 extending to 50° off-zenith, corresponding to a ~140-km horizontal averaging at 90 km altitude.

243 **4 Tidal Winds**

244 **a. Diurnal tide**

245 Time-height cross sections of daily diurnal tide zonal and meridional wind amplitudes
246 over DrAAMER during April, May, and June 2011 are displayed in the second panels of Figure
247 3 (at left and right, respectively). Monthly-mean diurnal tide amplitudes and phases over
248 DrAAMER and SAAMER (red and blue, respectively) are shown together for April, May, and
249 June (top to bottom) in Figure 7. Zonal and meridional components are shown at left and right,
250 and results for 2010 and 2011 are shown with solid and dashed lines, respectively. Black lines in
251 each panel are predictions by the GSWM-09 model.

252 Clearly seen in the daily cross sections in Figure 3 are amplitudes and temporal
253 variability similar to those reported earlier over SAAMER by *F10a*. These panels indicate
254 relatively small amplitudes in general, with maxima approaching $\sim 15 \text{ ms}^{-1}$ intermittently
255 occurring primarily at the highest altitudes. Monthly-mean amplitudes and phases for
256 DrAAMER and SAAMER shown together in Figure 7 reveal close agreement between the two
257 radars and between 2010 and 2011, except where amplitudes are small, $\sim 2 \text{ ms}^{-1}$ or smaller. These
258 differences are confined to the lower altitudes over SAAMER and the higher altitudes over
259 DrAAMER during June of 2010.

260 Comparing our observations with GSWM-09 predictions at 57°S , 65°W (approximately
261 midway between SAAMER and DrAAMER), we see that amplitude predictions agree very
262 well, in general, with measurements at both radars, with slight under-estimates of measured
263 amplitudes at $\sim 95 \text{ km}$ and above during April and other predictions within the standard
264 deviations of individual monthly estimates at lower altitudes during April and at most altitudes
265 during May and June. Phase predictions by GSWM-09 agree well with measurements over
266 DrAAMER during April in both years up to $\sim 95 \text{ km}$, but exhibit phase delays of several hours at
267 middle and higher altitudes compared to SAAMER measurements in both years. GSWM-09
268 phase predictions are likewise delayed relative to measurements during May and June by
269 typically $\sim 5\text{-}10 \text{ hr}$, with better agreement occurring at lower altitudes.

270 **b. Semidiurnal tide**

271 Time-height cross sections of daily semidiurnal tide zonal and meridional amplitudes
272 over DrAAMER during April, May, and June 2011 are displayed in the lower panels of Figure 3
273 (at left and right, respectively). Similar data for 2010 are not shown due to five ~ 3 to 10-day data
274 gaps that preclude a complete analysis of the short-term variability of these motions. Time-height

275 cross sections of daily semidiurnal tide zonal and meridional amplitudes (at left and right,
276 respectively) over SAAMER during April, May, and June of 2009, 2010, and 2011 (top to
277 bottom) are displayed in Figure 8 for comparison with measurements over DrAAMER. Because
278 of the high correlation between temporal variations of the semidiurnal tides over SAAMER and
279 DrAAMER during 2011, these fields illustrate the intra- and inter-annual variability of the
280 semidiurnal tides over both radars spanning the maximum response occurring in May of each
281 year [see *F10a*]. S-transforms of the daily semidiurnal tide amplitudes over SAAMER for each
282 year are shown in the upper and lower left three panels of Figure 9, with those over DrAAMER
283 for 2011 shown in the right panels. Monthly-mean semidiurnal tide amplitudes and phases over
284 DrAAMER and SAAMER (red and blue, respectively) are shown together for April, May, and
285 June (top to bottom) in Figure 10. As for the diurnal tide in Figure 7, zonal and meridional
286 components are shown at left and right, and results for 2010 and 2011 are shown with solid and
287 dashed lines, respectively. Black lines in each panel are predictions by the GSWM-09 model.

288 The daily amplitude cross sections in Figure 8 exhibit broad maxima extending from
289 ~mid April to mid June each year, meridional amplitudes typically exceeding zonal amplitudes,
290 and significant intra- and inter-annual variability in these responses. For example, meridional
291 amplitudes exceeding 60 ms^{-1} extend from ~mid April to mid June in 2009, but are largely
292 confined to ~mid April to mid May in 2010 and 2011. Notable, however, is the very high
293 correlation between the daily semidiurnal responses over SAAMER and DrAAMER during 2011
294 displayed in the lower panels of Figures 3 and 8. In all cases, maximum responses occur at the
295 highest altitudes and approach amplitudes of $\sim 70 \text{ ms}^{-1}$. Also seen on examination of Figures 2
296 and 8 is a tendency for semidiurnal tide amplitudes to be significantly anti-correlated with the
297 corresponding mean winds (zonal and meridional tide amplitude maxima appear correlated with

298 more westward or southward mean winds, respectively). This tendency is seen both for shorter-
299 duration maxima in the zonal component and for more extended intervals in the meridional
300 component, with the latter more conspicuous in the cross sections.

301 Temporal variability of semidiurnal tide amplitudes discussed in connection with Figures
302 3 and 8 is quantified with S-transforms of these data in Figure 9. Comparing the tidal results in
303 Figure 9 with the mean wind S-transforms in Figure 4, we see much more significant correlations
304 between tidal components exhibiting specific periodicities from ~5 to 20 days, as expected given
305 the shorter intrinsic time scales of the tides compared to PWs. As described by *F10a*, tidal
306 amplitudes exhibit significant variability at expected PW periods as well as longer-period
307 oscillations, and the dominant periodicities are typically seen to occur nearly simultaneously in
308 both tidal components. This is also seen to be the case over the three months during which the
309 semidiurnal tide achieves its maximum amplitudes throughout the year. Examples of strong
310 correlations at specific periodicities include

- 311 1) the two maxima at ~10 to 12 and 20 days in early April 2009,
- 312 2) the maxima at ~7 to 8 days in mid to late May and June 2009,
- 313 3) the ~10 to 12 day maxima in late April 2010,
- 314 4) the maxima at ~12 to 15 days throughout June 2010, and
- 315 5) the multiple maxima at ~8 to 15 days in late May and early June 2011 apparently
316 following longer periods at earlier times.

317 Clear correlations between tides over SAAMER and DrAAMER during 2011 are seen at periods
318 of ~5 to 8 days in April and early May and from ~8 to 20 days in late May and June. Each of the
319 maxima suggest significant tidal modulation by, or interactions with, the corresponding PW.

320 What is not seen in Figure 9 is evidence of strong tidal amplitude modulation when these
321 amplitudes are largest. Note, for example, that *the peaks in the S-transforms of semidiurnal tide*
322 *amplitudes shown in Figure 9 occur in all cases where tidal amplitudes are small.* The lack of
323 maxima in the S-transforms of tidal amplitudes implies a lack of variability, not small tidal
324 amplitudes. Instead, S-transform peaks accompany growth or decay of tidal amplitudes, and
325 suggest that PW interactions may play key roles at these times.

326 Monthly-mean semidiurnal tide amplitudes and phases over DrAAMER and SAAMER
327 shown together in Figure 10 reveal close agreement between the two radars each year and
328 between 2010 and 2011, in most cases. Amplitudes typically increase by factors of ~ 3 from 78 to
329 99 km in April and May of each year, with a cessation of growth with altitude above ~ 90 km
330 during June of each year. Amplitude profiles are nearly identical for both radars and both years
331 in April, while phases agree between radars, but differ by ~ 5 hr between 2010 and 2011.
332 Amplitudes in May and June agree better in the two years over each radar, but are ~ 20 to 50%
333 larger over SAAMER than over DrAAMER each year. Unlike phases in April, those in May and
334 June are in close agreement for both radars and years, except at the lowest altitudes during May
335 where amplitudes are very small. The distinct seasonal maximum over SAAMER in May noted
336 by *F10a* is seen to also occur over DrAAMER, though with a slightly weaker and lower
337 maximum amplitude in each component.

338 Comparing our semidiurnal tide observations with GSWM-09 predictions at 57°S , 65°W
339 (as above), we see that amplitude predictions agree very well during April below ~ 90 km, with
340 observed amplitudes larger by ~ 30 to 50% at higher altitudes. In contrast, GSWM-09 predictions
341 are typically ~ 3 to 5 times smaller than observed amplitudes during May and June. They are also
342 smaller than the GSWM-09 predictions in April, while observed amplitudes are larger, except

343 during June at the highest altitude. GSWM-09 predictions of semidiurnal tide phases differ
344 dramatically from our observations during April and May, being more nearly in anti-phase than
345 in-phase at both sites, despite the significant phase differences between years during April.
346 GSWM-09 predictions are, however, in reasonable agreement with measurements at both radars
347 during June up to ~90 km, above which they diverge and lead observations by ~4 hr at 99 km.

348 **5 GW Momentum Fluxes**

349 Monthly-mean GW momentum fluxes over the two radars are displayed in Figure 11.
350 The various panels show zonal and meridional fluxes (left and right) over DrAAMER and
351 SAAMER (red and black) for April, May, and June (top to bottom) of 2010 and 2011 (solid and
352 dashed lines), respectively. Momentum fluxes are shown from 79.5 to 91.5 km, as we have less
353 confidence in momentum flux estimates where meteor counts are small and at the highest
354 altitudes because large semidiurnal tides may introduce significant uncertainties.

355 Monthly-mean momentum fluxes displayed in Figure 11 exhibit considerable consistency
356 between 2010 and 2011 at altitudes of 91.5 km and below, within the expected uncertainties of
357 these measurements of $\sim 10 \text{ m}^2 \text{ s}^{-2}$ assessed by *F10b*. Zonal momentum fluxes are all close to zero
358 over the 79.5 to 91.5-km altitude range, with estimates for both radars at most times spread
359 nearly symmetrically about zero, again within the expected uncertainties. Meridional momentum
360 fluxes, in contrast, exhibit consistency between 2010 and 2011 and apparently systematic
361 variations from April to June of each year. Meridional momentum fluxes over SAAMER
362 increase from relatively small values of ~ 10 to $20 \text{ m}^2 \text{ s}^{-2}$ at 79.5 km in these months each year in
363 altitude and with time, with mean values for 2010 and 2011 of ~ 20 , 30, and $40 \text{ m}^2 \text{ s}^{-2}$ at 91.5 km.
364 Similar increases are seen to occur over DrAAMER at the higher altitudes (reaching $\sim 50 \text{ m}^2 \text{ s}^{-2}$ at

365 91.5 km in June), but with momentum fluxes at the lowest altitudes decreasing from near zero in
366 April to $\sim -20 \text{ m}^2\text{s}^{-2}$ in June.

367 Zonal momentum fluxes shown in Figure 11 are too close to zero and without clear
368 trends (within our expected uncertainties) to provide useful guidance on the potential GW
369 sources and filtering processes influencing zonal GW propagation at these altitudes. Meridional
370 momentum fluxes, however, are sufficiently non-zero to provide some useful guidance. At lower
371 altitudes, increasingly negative momentum fluxes over DrAAMER from April to June suggest
372 either 1) increasing sources of GWs propagating to the south below ~ 85 km and/or 2) more
373 favorable filtering conditions enabling increasing southward propagation with time. At the higher
374 altitudes, meridional momentum fluxes over DrAAMER and SAAMER increase northward with
375 time, suggesting a prevalence of GWs propagating northward at ~ 85 km and above over both
376 sites. Taken together, these results suggest increasing sources of GWs propagating meridionally
377 over the Drake Passage during April, May, and June of each year, with other dynamics somehow
378 removing the southward-propagating GWs from the spectrum at ~ 85 km and above or enhancing
379 the GWs propagating northward at these altitudes.

380 **6 Discussion**

381 **a. Mean winds**

382 Mean winds observed over DrAAMER and SAAMER during April to June of 2010 and
383 2011 discussed above are generally consistent with our previous measurements over SAAMER
384 [*F10a*, *F11a*] and with other assessments of inter-hemispheric mean winds at high latitudes
385 [*Avery et al.*, 1989; *Portnyagin et al.*, 2004, 2006; *Dowdy et al.*, 2007]. In particular, monthly-
386 mean zonal winds approaching winter are more strongly eastward over DrAAMER and
387 SAAMER at higher altitudes than at comparable northern latitudes. Monthly-mean meridional

388 winds are near zero or weakly poleward throughout our current observations, except over both
389 radars during June 2010, where weakly positive winds ($< 3 \text{ ms}^{-1}$) were observed below $\sim 90 \text{ km}$.
390 These inter-annual fluctuations are nevertheless within the range of variability imposed by PW
391 and longer-period modulations of these monthly means over both radars. The systematically-
392 stronger monthly-mean zonal winds at these locations, however, appear to be a consequence of
393 the unique large-scale dynamics accompanying the Drake Passage “hotspot” of enhanced GW
394 activity discussed at length by *F10a* and *F10b* and references cited above.

395 **b. Diurnal tide**

396 Diurnal tide assessments in the present study have addressed only comparisons between
397 sites and inter-annual comparisons during April to June of 2010 and 2011. We can nevertheless
398 report on improvements in comparisons of current amplitude measurements with the newer
399 GSWM-09 model compared to GSWM-02 predictions. Our previous analysis by *F10a* compared
400 SAAMER measurements with GSWM-02 results and found GSWM-02 to systematically over-
401 estimate diurnal tide amplitudes over SAAMER. However, current diurnal tide amplitude
402 estimates over DrAAMER and SAAMER are in excellent agreement with GSWM-09 predictions
403 at all but the highest altitudes (95 km and above), due to reductions in the GSWM-09 amplitudes
404 relative to GSWM-02. Measured diurnal tide phases during April to June do not agree as well as
405 the GSWM-02 predictions, however, with systematic delays of predicted wind maxima relative
406 to our radar observations at both sites even at lower altitudes where previous comparisons with
407 SAAMER were very good (see Figure 7 and *F10a*, Figure 9).

408 **c. Semidiurnal tide**

409 Semidiurnal tide assessments in the present analysis are largely consistent with our
410 previous study employing SAAMER [*F10a*] in which annual maxima of monthly-mean

411 semidiurnal tide amplitudes were found to occur in May of each year. Significant inter-annual
412 variability is also apparent, however, as the monthly-mean diurnal amplitudes in the present
413 study over SAAMER are seen to vary from somewhat larger than during 2008 and 2009 to
414 significantly smaller (compare Figure 10 with *F10a*, Figure 11). Specifically, amplitudes at 99
415 km during April 2010 and 2011 are $\sim 10 \text{ ms}^{-1}$ smaller than previous years, amplitudes at 99 km
416 during May are comparable to previous years, while those during June are ~ 20 and 10 ms^{-1}
417 smaller than reported by *F10a* in 2010 and 2011, respectively.

418 Monthly-mean semidiurnal tide amplitudes are systematically smaller over DrAAMER
419 than over SAAMER during April, May, and June 2010 and 2011, with differences of ~ 5 to 20
420 ms^{-1} , though the vertical profiles and phase structures are in close agreement each year. They
421 appear to be similar, however, to those seen in the study of GW-tidal interactions employing the
422 meteor radar at Rothera (67.6°S , 68.1°W) by *Beldon and Mitchell* [2010], from which we
423 inferred May 2007 monthly-mean zonal and meridional amplitudes at ~ 97 km from composite-
424 day winds to be ~ 45 and 35 ms^{-1} (see their Figure 7), respectively.

425 Also noted in our examination of semidiurnal tide variability were 1) tendencies for
426 amplitudes to achieve maxima during times for which zonal and meridional winds were
427 minimum (more westward and southward, respectively) and 2) tendencies for the major
428 modulations of the semidiurnal tide at times at which amplitudes were relatively small.

429 **c. GW momentum fluxes**

430 GW momentum fluxes reported here span April, May, and June 2010 and 2011 over
431 DrAAMER and SAAMER, both of which are within the Drake Passage “hotspot” of GW
432 activity seen during Austral winter to host the strongest stratospheric GW temperature variances
433 observed at any site on Earth [*Jiang et al.*, 2002, 2006; *Eckermann et al.*, 2006]. *F10b* observed

434 GW momentum fluxes in the MLT over SAAMER during November 2008 and March 2009 that
435 exhibited anti-correlations with mean zonal winds that were consistent with observations at other
436 sites ranging from middle to high latitudes, including the MF radar in Australia [*Vincent and*
437 *Reid*, 1983; *Reid and Vincent*, 1986; *Fritts and Vincent*, 1987], the former Poker Flat radar in
438 Alaska [*Fritts and Yuan*, 1989; *Wang and Fritts*, 1990, 1991], and the MU radar in Japan [*Tsuda*
439 *et al.*, 1990]. During Austral winter (June 2008 and 2009 and September 2008), however, zonal
440 momentum fluxes over SAAMER reported by *F10b* were more nearly correlated with the mean
441 zonal wind, and meridional momentum fluxes were likewise large and positive, suggesting GW
442 propagation eastward and northward away from the Drake Passage at these times.

443 *F10b* attributed the November 2008 and March 2009 anti-correlations of momentum
444 fluxes and mean zonal winds to the same GW filtering dynamics believed to account for these
445 correlations at other sites. The unusual relations between momentum fluxes and mean winds
446 (including the larger sustained eastward winds during Austral winter extending to higher
447 altitudes than seen at other sites, with corresponding poleward mean meridional winds occurring
448 at higher altitudes, see *F11a*) were attributed instead to the unique (but poorly understood)
449 dynamics of the Drake Passage “hotspot” and indications of a spectrum of GW sources including
450 jet streams with high eastward winds that might account for eastward GW phase speeds
451 extending into the MLT.

452 Our present DrAAMER and SAAMER observations are generally consistent with this
453 same picture of the MLT GW and mean flow dynamics. June 2010 and 2011 zonal momentum
454 fluxes are near zero at both sites, thus smaller than estimated over SAAMER in June 2008 or
455 2009, but comparable to those in March 2009. Mean zonal winds over SAAMER in June 2010
456 and 2011, however, are somewhat larger than seen over SAAMER in June 2008 and 2009 (by

457 $\sim 10 \text{ ms}^{-1}$). If filtering arguments are relevant to these dynamics, we would expect that stronger
458 eastward winds should contribute to the dissipation of GWs propagating eastward, thus reducing
459 eastward momentum fluxes relative to westward momentum fluxes and causing the net zonal
460 momentum flux to decrease, as seen in our current observations.

461 If a strong polar night jet at lower altitudes over the Drake Passage contributes GWs
462 having both significant eastward phase speeds and a range of propagation directions (as we
463 expect from spatially-localized jet stream forcing), then we should also expect that these GWs
464 will contribute to net northward propagation (and positive meridional momentum fluxes) over
465 SAAMER and net southward propagation (and negative meridional momentum fluxes) over
466 DrAAMER at higher altitudes, apart from additional filtering effects. Such a source would seem
467 to provide an explanation for the positive momentum fluxes over SAAMER and the negative
468 momentum fluxes over DrAAMER below $\sim 85 \text{ km}$. At present, however, we have no explanation
469 for why GW momentum fluxes should be positive over the two sites at the northern and southern
470 sides of the Drake passage above $\sim 85 \text{ km}$, although auroral heating is one possible source.

471 As noted by *F10b*, large GW momentum fluxes accompanying tidal modulation [*Fritts*
472 *and Vincent*, 1987; *Wang and Fritts*, 1991; *Espy et al.*, 2004], arising from specific sources [*Espy*
473 *et al.*, 2006; *Smith et al.*, 2009], or having no identified cause [*Fritts et al.*, 2002] readily occur in
474 the MLT. Momentum fluxes accompanying such events can significantly exceed the mean
475 values reported at various sites, occasionally by one or two decades. So it is not surprising that
476 large monthly mean GW momentum fluxes can also occur in regions of demonstrated strong
477 local GW sources, as appears to be the case over DrAAMER and SAAMER, especially during
478 austral winter when multiple strong sources are expected to occur. What remains to be explained
479 are the dynamics that lead to the large mean momentum fluxes observed over the Drake Passage

480 “hotspot” and their implications for the local and global structure and variability of the MLT in
481 this region.

482 7 **Summary and Conclusions**

483 We described in this paper a new meteor radar, the Drake Antarctic Agile MEteor Radar
484 (DrAAMER) located at Ferraz Station on King George Island (62.1°S, 58.7°W), which, like its
485 predecessor SAAMER located at Rio Grande on Tierra del Fuego (53.8°S, 67.8°W), was
486 designed to enable high resolution wind measurements for assessments of mean, PW, and tidal
487 wind fields, a capability for assessing GW momentum fluxes, and advanced meteor studies.
488 DrAAMER was installed and became operational in March 2010.

489 To evaluate DrAAMER performance and begin to characterize the large- and smaller-
490 scale dynamics of the Drake Passage “hotspot” more fully, we also described the mean and tidal
491 wind fields and GW momentum flux estimates over DrAAMER during April, May, and June of
492 2010 and 2011, performed comparisons with correlative measurements by SAAMER, and
493 compared tidal wind measurements at both sites with the newer GSWM-09 model.

494 Daily-mean zonal and meridional winds were found to agree closely between the two
495 sites during April, May, and June 2011 for which correlative data were available. They were also
496 found to exhibit similar structure and variability as seen during 2008 and 2009 over SAAMER.
497 S-transforms of these winds revealed dominant periodicities at both sites corresponding to
498 various PW and longer-period oscillations. Primary responses were seen at ~5 to 15 days
499 throughout the 3-month data set, ~20 to 30 days at the beginning and end of the data set, and ~30
500 to 45 days in the latter portion of the data set. These various responses were somewhat correlated
501 between sites and somewhat stronger in the zonal wind over SAAMER. There was also
502 variability, however, suggesting a delayed response at one site relative to the other or a

503 significant response in one wind component that had a small or no response in the other
504 component. Both the daily-mean wind cross sections and their S-transforms for SAAMER
505 revealed significant inter-annual variability in the 3-month interval examined each year.

506 Monthly-mean winds were seen to agree closely between sites, with maximum
507 differences of $\sim 5 \text{ ms}^{-1}$. Differences are expected in both the zonal and meridional mean winds at
508 high latitudes, as the zonal jet must decrease towards the pole, and the mean meridional
509 circulation is determined by latitudinally-varying GW forcing of the MLT. However, other
510 factors also appear to contribute to the differences observed in our study. These include 1) the
511 large PW and longer-period oscillations seen in the daily-mean winds, 2) the lack of exact
512 phasing of these various modulations at the two sites, and 3) data gaps, especially for DrAAMER
513 during 2010, which presumably cause incomplete averaging over the various oscillations
514 influencing each monthly mean.

515 Tides, especially the semidiurnal tide, are seen to make dominant contributions to the
516 large-scale wind fields. The diurnal tide contributes winds typically of $\sim 5 \text{ ms}^{-1}$ at most altitudes,
517 with maxima approaching $\sim 10 \text{ ms}^{-1}$, except at the highest altitudes where daily amplitudes may
518 be twice as large. Semidiurnal tide zonal and meridional winds, in contrast, contribute very
519 significantly to the motion field over both radars, with monthly-mean amplitudes typically
520 approaching ~ 20 to 50 ms^{-1} at the highest altitudes, with maxima of $\sim 65 \text{ ms}^{-1}$ in the meridional
521 component over SAAMER in June and daily amplitudes exceeding $\sim 70 \text{ ms}^{-1}$. Semidiurnal tide
522 amplitudes are typically ~ 20 to 50% larger over SAAMER than over DrAAMER each year.
523 They also tend to be anti-correlated with eastward and northward winds and to exhibit the
524 greatest variability at various PW periods when amplitudes are small.

525 Our limited analysis also suggests little inter-annual variability of monthly-mean
526 semidiurnal tide amplitudes over SAAMER during April and May and over DrAAMER during
527 April and June of 2010 and 2011, with greater inter-annual variability over DrAAMER during
528 May and at lower altitudes, and over SAAMER during June. Semidiurnal phases compare
529 closely between the two sites in both components each year, but exhibit greater inter-annual
530 variability in April than in May or June (phase differences of ~2 to 3 hr in April and ~1 hr or less
531 in May and June). Phase progression is downward and relatively uniform in altitude, implying
532 upward propagation and a vertical wavelength of ~60 to 80 km. Semidiurnal tide amplitudes are
533 systematically larger than predictions by the GSWM-09 model, with the largest discrepancies
534 occurring in May and June. Significant phase discrepancies are also observed, being more nearly
535 in anti-phase during April and May, but in-phase below ~90 km in June, with departures
536 increasing at higher altitudes implying a shorter predicted vertical wavelength than observed.

537 Our analysis of GW momentum fluxes during April, May, and June 2010 and 2011
538 revealed significant consistency between sites and years, as well as with the general findings by
539 *F10b* over SAAMER in 2008 and 2009, but significant departures from mean wind and
540 momentum flux correlations widely reported elsewhere and also seen over SAAMER except in
541 Austral winter. These differences were attributed to the expected unique (but poorly understood)
542 dynamics of the Drake Passage “hotspot” and indications of a spectrum of GW sources including
543 jet streams with high eastward winds that might account for eastward GW phase speeds
544 extending into the MLT and the stronger eastward mean winds in this region than seen at
545 comparable northern latitudes. Our inferred GW momentum fluxes exhibited zonal mean values
546 near zero (within our estimation uncertainties), suggesting a balance between eastward and
547 westward GW momentum transport that is consistent with the lack of significant zonal mean

548 wind variations with altitude. Significant differences were seen in the mean meridional
549 momentum fluxes over SAAMER and DrAAMER, with negative and positive fluxes,
550 respectively, below ~85 km approaching Austral winter, and positive fluxes over both radars at
551 higher altitudes. The momentum flux variations at lower altitudes were considered to be
552 consistent with possible jet stream sources primarily over the Drake Passage, with dominant GW
553 propagation northward and southward over SAAMER and DrAAMER, respectively.

554 We have no explanation at present for the increasing positive meridional momentum
555 fluxes at higher altitudes, and the corresponding implied equatorward GW propagation. Auroral
556 GW generation is one possibility, but there are no measurements of momentum fluxes in polar
557 winter at these altitudes (even the Poker Flat radar was unable to make measurements in winter
558 above ~85 km), nor are there modeling studies that predict GW responses to auroral forcing.
559 Thus, an explanation will need to await further quantification of these dynamics.

560

561 **Acknowledgments** The acquisition and installation of DrAAMER, and the research described in
562 this paper, were performed under NSF grant OPP-0839084. We are especially grateful to the
563 Secretaria for the Interministerial Commission of Sea Resources (SECIRM) and the Brazilian
564 Antarctic Program (PROANTAR) for their support of this research and visits to Ferraz Station
565 required by project personnel to install and service DrAAMER. The authors are also very
566 grateful for the valuable support of personnel at Estacion Astronomica Rio Grande (EARG) for
567 their assistance with the operations and maintenance of SAAMER. Finally, we are indebted to
568 MARDOC and Genesis Software for working with us to devise a radar configuration that met
569 our measurement objectives. We also acknowledge use of the CEDAR database and the GSWM-
570 09 website at NCAR for GSWM-09 results employed for our comparisons.

571 **8 References**

- 572 Alexander, M. J., J. Gille, J. C. Cavanaugh, et al., 2008a: Global estimates of gravity wave
573 momentum flux from High Resolution Dynamics Limb Sounder observations, *J. Geophys.*
574 *Res.*, 113, D15S18, doi:10.1029/2007JD008807.
- 575 Alexander, M. J., Teitelbaum, H., Eckermann, S. D., Gille, J., Barnett, J., and Barnett, C., 2008b:
576 High-resolution satellite observations of mountain waves, *B. Am. Meteor. Soc.*, 89, 151–152.
- 577 Avery, S. K., R. A. Vincent, A. Phillips, A. H. Manson, and G. J. Fraser, 1989: High-latitude
578 tidal behavior in the mesosphere and lower thermosphere, *J. Atmos. Terres. Phys.*, 51 (7/8),
579 595-608.
- 580 Beldon, C. L., and N. J. Mitchell, 2010: Gravity wave–tidal interactions in the mesosphere and
581 lower thermosphere over Rothera, Antarctica (68°S, 68°W), *J. Geophys. Res.*, 115, D18101,
582 doi:10.1029/2009JD013617.
- 583 Burrage, M. D., M. E. Hagan, W. R. Skinner, D. L. Wu, and P. B. Hays, 1995: Long-term
584 variability in the solar diurnal tide observed by HRDI and simulated by the GSWM,
585 *Geophys. Res. Lett.*, 22(19), 2641–2644.
- 586 Dowdy, A. J., R. A. Vincent, M. Tsutsumi, K. Igarashi, Y. Murayama, W. Singer, and D. J.
587 Murphy, 2007: Polar mesosphere and lower thermosphere dynamics: 1. Mean wind and
588 gravity wave climatologies, *J. Geophys. Res.*, 112, D17104, doi:10.1029/2006JD008126.
- 589 Eckermann, S. D., and C. J. Marks, 1996: An Idealized Ray Model of Gravity Wave-Tidal
590 Interactions, *J. Geophys. Res.*, 101(D16), 96JD01660, 21,195-21,212.
- 591 Eckermann, S. D., D. L. Wu, J. D. Doyle, J. F., Burris, T. J. McGee, C. A. Hostetler, L. Coy, B.
592 N. Stephens, J. P. McCormack, and T. F. Hogan, 2006: Imaging gravity waves in lower
593 stratospheric AMSU-A radiances, Part 2: Validation case study, *Atmos. Chem. Phys.*, 6,

594 3343–3362.

595 Ern, M., P. Preusse, M. J. Alexander, and C. D. Warner, 2004: Absolute values of gravity wave
596 momentum flux derived from satellite data, *J. Geophys. Res.*, 109, D20103,
597 doi:10.1029/2004JD004752, 2004.

598 Espy, P. J., R. E. Hibbins, G. R. Swenson, J. Tang, M. J. Taylor, D. M. Riggin, and D. C. Fritts,
599 2006: Regional variations of mesospheric gravity wave momentum fluxes over Antarctica,
600 *Ann. Geophys.*, 24, SRef-ID: 1432-0576/ag/2006-24-81, 81-88.

601 Espy, P. J., G. O. L. Jones, G. R. Swenson, J. Tang and M. J. Taylor, 2004: Tidal modulation of
602 the gravity-wave momentum flux in the Antarctic mesosphere, *Geophys. Res. Lett.*, 31,
603 L11111, doi:10.1029/2004JGLO19624.

604 Forbes, J. M., 1995: Tidal and planetary waves, *The upper mesosphere and lower thermosphere:*
605 *a review of experiment and theory*, R. M. Johnson and T. L. Killeen, Eds., AGU Monograph.

606 Forbes, J. M., and J. Gu, and S. Miyahara, 1991: On the interactions between gravity waves and
607 the diurnal propagating tide. *Planet. Space Sci.*, 39, 1249-1257.

608 Fritts, D. C., and M. J. Alexander, 2003: Gravity dynamics and effects in the middle
609 atmosphere, *Rev. Geophys.*, 41, doi:10.1029/2001RG000106.

610 Fritts, D. C., H. Iimura, R. Lieberman, D. Janches, and W. Singer, 2011a: A Conjugate Study of
611 Mean Winds and Planetary Waves Employing Enhanced Meteor Radars at Rio Grande,
612 Argentina (53.8oS) and Juliusruh, Germany (54.6oN), *J. Geophys. Res.*, submitted.

613 Fritts, D. C., D. Janches, and W. K. Hocking, 2011b: Assessment of gravity wave momentum
614 flux measurement capabilities by meteor radars having different transmitter power and
615 antenna configurations, *J. Geophys. Res.*, to be submitted.

616 Fritts, D. C., D. Janches, H. Iimura, W. K. Hocking, N. J. Mitchell, B. Fuller, B. Vandeppeer, J.
617 Hormaechea, C. Brunini, and H. Levato, 2010a: Southern Argentina agile meteor radar
618 (SAAMER): System design and initial measurements of large-scale winds and tides, J.
619 Geophys. Res., 115, D18112, doi:10.1029/2010JD013850.

620 Fritts, D. C., D. Janches, and W. K. Hocking, 2010b: Southern Argentina agile meteor radar
621 (SAAMER): Initial assessment of gravity wave momentum fluxes, J. Geophys. Res., 115,
622 D19123, doi:10.1029/2010JD013891.

623 Fritts, D. C., T. Tsuda, T. E. VanZandt, S. A. Smith, T. Sato, S. Fukao, and S. Kato, 1990:
624 Studies of velocity fluctuations in the lower atmosphere using the MU radar: II. Momentum
625 fluxes and energy densities. J. Atmos. Sci., 47, 51-66.

626 Fritts, D. C., S. A. Vadas, and Y. Yamada, 2002: An estimate of strong local gravity wave body
627 forcing based on OH airglow and meteor radar observations, Geophys. Res. Lett., 29 (10),
628 10.1029/2001GL013753.

629 Fritts, D. C., and R. A. Vincent, 1987: Mesospheric momentum flux studies at Adelaide,
630 Australia: Observations and a gravity wave/tidal interaction model, J. Atmos. Sci., 44, 605-
631 619.

632 Fritts, D. C., and L. Yuan, 1989: Measurement of momentum fluxes near the summer
633 mesopause at Poker Flat, Alaska, J. Atmos. Sci., 46, 2569-2579.

634 Hagan, M. E., M. D. Burrage, J. M. Forbes, J. Hackney, W. J. Randel, and X. Zhang, 1999:
635 GSWM-98: Results for migrating solar tides, J. Geophys. Res., 104(A4), 6813-68-27.

636 Hagan, M. E. and J. M. Forbes, 2002: Migrating and nonmigrating diurnal tides in the middle
637 and upper atmosphere excited by tropospheric latent heat release, J. Geophys. Res.,
638 107(D24), 4754, doi: 10.1029/2001JD001236.

639 Hagan, M. E., and J. M. Forbes, 2003: Migrating and nonmigrating semidiurnal tides in the
640 upper atmosphere excited by tropospheric latent heat release, *J. Geophys. Res.*, 108(A2),
641 1062, doi:10.1029/2002JA009466.

642 Hertzog, A., G. Boccara, R. A. Vincent, F. Vial, and P. Cocquerez, 2008: Estimation of gravity
643 wave momentum flux and phase speeds from quasi-Lagrangian stratospheric balloon flights.
644 Part II: Results from the Vorcore campaign in Antarctica, *J. Atmos. Sci.*, 65, 3056–3070.

645 Holton, J. R., 1984: The generation of mesospheric planetary waves by zonally asymmetric
646 gravity wave breaking. *J. Atmos. Sci.*, 41, 3427-3430.

647 Isler, J.R., and D. C. Fritts, 1996. Gravity wave variability and interactions with lower-frequency
648 motions in the mesosphere and lower thermosphere over Hawaii, *J. Atmos. Sci.*, 53, 37-48.

649 Jiang, J. H., S. D. Eckermann, D. L. Wu, D. Y. Wang, 2006: Inter-annual variation of gravity
650 waves in the Arctic and Antarctic winter middle atmosphere, *Adv. Space Res.*, 37, 2418-
651 2423.

652 Jiang, J. H., D. L. Wu, and S. D. Eckermann, 2002: Upper Atmosphere Research Satellite
653 (UARS) MLS observation of mountain waves over the Andes, *J. Geophys. Res.*, 107, D20,
654 8273, doi:10.1029/2002JD002091.

655 Jones, J., A.R. Webster, and W.K. Hocking, 1998: An improved interferometer design for use
656 with meteor radars, *Radio Sci.*, 33, 55-65.

657 Lieberman, R. S., J. Oberheide, M. E. Hagan, E. E. Remsberg, and L. L. Gordley, 2004:
658 Variability of diurnal tides and planetary waves during November 1978–May 1979, *J.*
659 *Atmos. Solar-Terres. Phys.*, 66(6-9), 517-528, doi:10.1016/j.jastp.2004.01.006.

660 Liu, X., J. Xu, H.-L. Liu, and R. Ma, 2008: Nonlinear interactions between gravity waves with
661 different wavelengths and diurnal tide, *J. Geophys. Res.*, 113, D08112,

662 doi:10.1029/2007JD009136.

663 Lu, W., and D. C. Fritts, 1993: Spectral estimates of gravity wave energy and momentum fluxes,
664 III: Gravity wave-Tidal interactions. *J. Atmos. Sci.*, 50, 3714-3727.

665 Manson, A.H., C.E. Meek, and G. E. Hall, 1998. Correlations of gravity waves and tides in the
666 mesosphere over Saskatoon. *J. Atmos. Solar-Terres. Phys.*, 60, 1089–1107.

667 Manson, A. H, C. Meek, M. Hagan, C. Hall, W. Hocking, J. MacDougall, S. Franke, D. Rigglin,
668 D. Fritts, R. Vincent, and M. Burrage, 1999: Seasonal variations of the semi-diurnal and
669 diurnal tides in the MLT: multi-year MF radar observations from 2 to 70°N, and the GSWM
670 tidal model, *J. Atmos. Solar-Terres. Phys.*, 61(11), 809-828, doi:10.1016/S1364-
671 6826(99)00045-0.

672 McLandress, C., 1998: On the importance of gravity waves in the middle atmosphere and their
673 parameterization in general circulation models, *J. Atmos. Solar-Terr. Phys.*, 60, 1357-1383.

674 McLandress, C., 2002: The seasonal variation of the propagating diurnal tide in the mesosphere
675 and lower thermosphere. Part I: The role of gravity waves and planetary waves. *J. Atmos.*
676 *Sci*, 59:5, 907-922.

677 McLandress, C., M. J. Alexander and D. L. Wu, 2000: Microwave Limb Sounder observations
678 of gravity waves in the stratosphere: A climatology and interpretation, *J. Geophys. Res.*,
679 105(D9), 11,947-11,967.

680 McLandress, C., and W. E. Ward, 1994: Tidal/gravity wave interactions and their influence on
681 the large-scale dynamics of the middle atmosphere: Model results, *J. Geophys. Res.*, 99,
682 8139-8156.

683 Meyer, C. K., 1999: Gravity wave interactions with the diurnal propagating tide. *J. Geophys.*
684 *Res.*, 104, 4223-4239.

685 Miyahara, S., 1985: Suppression of stationary planetary waves by internal gravity waves in the
686 mesosphere. *J. Atmos. Sci.*, 42, 100-107.

687 Miyahara, S., Y. Hayashi, and J.D. Mahlman, 1986: Interactions between gravity waves and
688 planetary-scale flow simulated by the GFDL “SKYHI” general circulation model. *J. Atmos.*
689 *Sci.*, 43, 1844-1861.

690 Murphy, D. J., J. M. Forbes, R. L. Walterscheid, M. E. Hagan, S. K. Avery, T. Aso, G. J. Fraser,
691 D. C. Fritts, M. J. Jarvis, A. J. McDonald, D. M. Riggin, M. Tsutsumi, and R. A. Vincent,
692 2006: A climatology of tides in the Antarctic mesosphere and lower thermosphere, *J.*
693 *Geophys. Res.*, 111, D23104, doi:10.1029/2005JD006803.

694 Murphy, D. J., and R. A. Vincent, 1998: Mesospheric momentum fluxes over Adelaide during
695 the 2-day wave: Results and interpretation, *J. Geophys. Res.*, 103, 28,627-28,636.

696 Pancheva, D., N. J. Mitchell, M. E. Hagan, A. H. Mansons, C. E. Meek, Yi Luo, Ch. Jacobi, D.
697 Kürschner, R. R. Clark, W. K. Hocking, J. MacDougall, G. O. L. Jones, R. A. Vincent, I. M.
698 Reid, W. Singer, K. Igarashi, G. I. Fraser, T. Nakamura, T. Tsuda, Yu. Portnyagin, E.
699 Merzlyakov, A. N. Fahrutdinova, A. M. Stepanov, L. M. G. Poole, S. B. Malinga, B. L.
700 Kashcheyev, A. N. Oleynikov, D. M. Riggin, 2002: Global-scale tidal structure in the
701 mesosphere and lower-thermosphere during the PSMOS campaign of June-August 1999 and
702 comparisons with the global-scale wave model, *J. Atmos. Solar-Terres. Phys.*, 64, 1011-
703 1035.

704 Pancheva, D., N. J. Mitchell, A. H. Manson, et al., 2004: Variability of the quasi-2-day wave
705 observed in the MLT region during the PSMOS campaign of June–August 1999, *J. Atmos.*
706 *Solar-Terres. Phys.*, 66, doi:10.1016/j.jastp.2004.01.008, 539-565.

707 Pancheva, D., P. Mukhtarov, and B. Andonov, 2009: Global structure, seasonal and interannual
708 variability of the migrating semidiurnal tide seen in the SABER/TIMED temperatures (2002-
709 2007), *Ann. Geophys.*, *27*, 687-703.

710 Portnyagin, Yu. I., E. G. Merzlyakov, T. V. Solov'eva, N.A. Makarov, 2006: Interhemispheric
711 distinctions in wind-regime parameters in the polar mesosphere-lower thermosphere,
712 *Izvestiya, Atmos. Oceanic Phys.*, *42*(1), 93-104.

713 Portnyagin, Yu., T. Solovjova, E. Merzlyakov, et al., 2004: Mesosphere/lower thermosphere
714 prevailing wind model, *Adv. Space Res.*, *34*, 1755-1762.

715 Preusse, P., A. Dornbrack, S. D. Eckermann, M. Riese, B. Schaeler, J. T. Bacmeister, D.
716 Broutman, and K. U. Grossmann, 2002: Space based measurements of stratospheric
717 mountain waves by CRISTA, 1. Sensitivity, analysis method and a case study, *J. Geophys.*
718 *Res.*, *107*, 8178, doi:10.1029/2001JD000699.

719 Preusse, P., S.D. Eckermann, J. Oberheide, M.E. Hagan, and D. Offermann, 2001: Modulation
720 of gravity waves by tides as seen in CRISTA temperatures, *Adv. Space Res.*, *27* (10), 1773-
721 1778.

722 Preusse, P., M. Ern, S. D. Eckermann, C. D. Warner, R. H. Picard, P. Knieling, M. Krebsbach, J.
723 M. Russell III, M. G. Mlynczak, C. J. Mertens, and M. Riese, 2006: Tropopause to
724 mesopause gravity waves in August: Measurement and modeling, *J. Atmos. Sol.-Terr. Phys.*,
725 *68*, 1730–1751.

726 Smith, S., J. Baumgardner, and M. Mendillo, 2009: Evidence of mesospheric gravity-waves
727 generated by orographic forcing in the troposphere, *J. Geophys. Res.*, **36**, L08807,
728 doi:10.1029/2008GL036936.

729 Stockwell, R. G., L. Mansinha, and R. Lowe, 1996: Localization of the complex spectrum: The S

730 transform, *IEEE Trans. Signal Process.*, 44(4), 998 – 1001.

731 Thayaparan, T., W.K. Hocking, and J. MacDougall, 1995. Observational evidence of
732 tidal/gravity wave interactions using the UWO 2MHz radar, *Geophys. Res. Lett.*, 22, 373-
733 376.

734 Tsuda, T., Y. Murayama, M. Yamamoto, S. Kato, and S. Fukao, 1990: Seasonal variation of
735 momentum flux in the mesosphere observed with the MU radar, *Geophys. Res. Lett.*, 17(6),
736 725–728, doi:10.1029/GL017i006p00725.

737 Tsuda, T., M. Nishida, C. Rocken, and R. H. Ware, 2000: A global morphology of gravity wave
738 activity in the stratosphere revealed by the GPS occultation data GPS/MET, *J. Geophys.*
739 *Res.*, 105, 7257–7273.

740 VanZandt, T. E., S. A. Smith, T. Tsuda, D. C. Fritts, T. Sato, S. Fukao, and S. Kato, 1990:
741 Studies of velocity fluctuations in the lower atmosphere using the MU radar. Part I:
742 Azimuthal anisotropy, *J. Atmos. Sci.*, 47(1), 39-50.

743 Vincent, R. A., S. Kovalam, D. C. Fritts, and J. R. Isler, 1998: Long-term MF radar observations
744 of solar tides in the low-latitude mesosphere: Interannual variability and comparisons with
745 the GSWM, *J. Geophys. Res.*, 103(D8), 8667–8683.

746 Vincent, R.A., and I. M. Reid, 1983. HF Doppler measurements of mesospheric momentum
747 fluxes. *Journal of Atmospheric Science*40, 1321–1333.

748 Wang, D.-Y., and D. C. Fritts, 1990: Mesospheric momentum fluxes observed by the MST radar
749 at Poker Flat, Alaska, *J. Atmos. Sci.*, 47, 1511-1521.

750 Wang, D.-Y., and D. C. Fritts, 1991: Evidence of gravity wave-tidal interaction observed near
751 the summer mesopause at Poker Flat, Alaska , *J. Atmos. Sci.*,48, 572-583.

752 Wu, D. L., 2004: Mesoscale gravity wave variances from AMSU-A radiances, *Geophys. Res.*
753 *Letts.*, 31, doi:10.1029/2004GL019562.

754 Wu., D. L., and S. D. Eckermann, 2008: Global Gravity Wave Variances from Aura MLS:
755 Characteristics and Interpretation, *J. Atmos. Sci.*, 65, 3695-3718, DOI:
756 10.1175/2008JAS2489.1.

757 Wu, D. L., and J. H. Jiang, 2002: MLS observations of atmospheric gravity waves over
758 Antarctica, *J. Geophys. Res.*, 107, NO. D24, 4773, doi:10.1029/2002JD002390.

759 Wu, D. L., P. Preusse, S. D. Eckermann, J. H. Jiang, M. de la Torre Juarez, L. Coy, D. Y. Wang,
760 2006: Remote sounding of atmospheric gravity waves with satellite limb and nadir
761 techniques, *Adv. Space Res.*, 37, 2269-2277.

762 Zhang, X.,J. M. Forbes, and M. E. Hagan, 2010a: Longitudinal variation of tides in the MLT
763 region: 1. Tides driven by tropospheric net radiative heating, *J. Geophys. Res. (Space*
764 *Physics)*, 115, 6316, doi:10.1029/2009JA014897.

765 Zhang, X.,J. M. Forbes, and M. E. Hagan, 2010b: Longitudinal variation of tides in the MLT
766 region: 2. Relative effectis of solar radiative and latent heating, *J. Geophys. Res. (Space*
767 *Physics)*, 115, 6317, doi:10.1029/2009JA014898.

768

769

770

771

772

773

774

775 **Figure captions**

776 **Figure 1.** (top) Unambiguous meteors detected by SAAMER (on Tierra del Fuego) and
777 DrAAMER (on King George Island) for one day showing the radar beam sensitivity. (bottom,
778 left) Daily unambiguous meteor counts over SAAMER/TdF during 2011 (solid) and
779 DrAAMER/KGI (dashed), and (bottom, right) meteor altitude distributions over each radar.

780 **Figure 2.** (left) Zonal and (right) meridional daily-mean winds over SAAMER for April, May,
781 and June of (top) 2009, (middle) 2010, and (bottom) 2011. Note the difference color scales in
782 each column.

783 **Figure 3.** (left) Zonal and (right) meridional (top) daily-mean winds, (middle) diurnal tide
784 amplitudes, and (bottom) semidiurnal tide amplitudes over DrAAMER for April, May, and June
785 of 2011. Note the difference color scales in each row.

786 **Figure 4.** S-transforms of (top) zonal and (bottom) meridional daily-mean winds for April, May,
787 and June (left to right) of 2009, 2010, and 2011, respectively, over SAAMER and for 2011 over
788 DrAAMER. Amplitudes at each frequency are shown with the color bars at right in each case.

789 **Figure 5.** Monthly-mean (left) zonal and (right) meridional winds for (top) April, (middle) May,
790 and (bottom) June of (solid lines) 2010 and (dashed lines) 2011 over (red) DrAAMER and (blue)
791 SAAMER. Standard deviations are shown with horizontal lines in each case.

792 **Figure 6.** Power spectra of hourly (top) zonal and (bottom) meridional winds during April, May,
793 and June 2011 over DrAAMER. Tidal peaks are indicated, and periods are shown from 2 hr to
794 ~40 days.

795 **Figure 7.** Diurnal tide (column 1) zonal and (column 3) meridional amplitudes and (column 2)
796 zonal and (column 4) meridional phases for (top) April, (middle) May, and (bottom) June of

797 (solid lines) 2010 and (dashed lines) 2011 over (red) DrAAMER and (blue) SAAMER. Standard
798 deviations are shown with horizontal lines in each case. Black lines show GSWM-09 predictions.

799 **Figure 8.** As in Figure 2, but for semidiurnal tide amplitudes.

800 **Figure 9.** As in Figure 4, but for semidiurnal tide amplitudes.

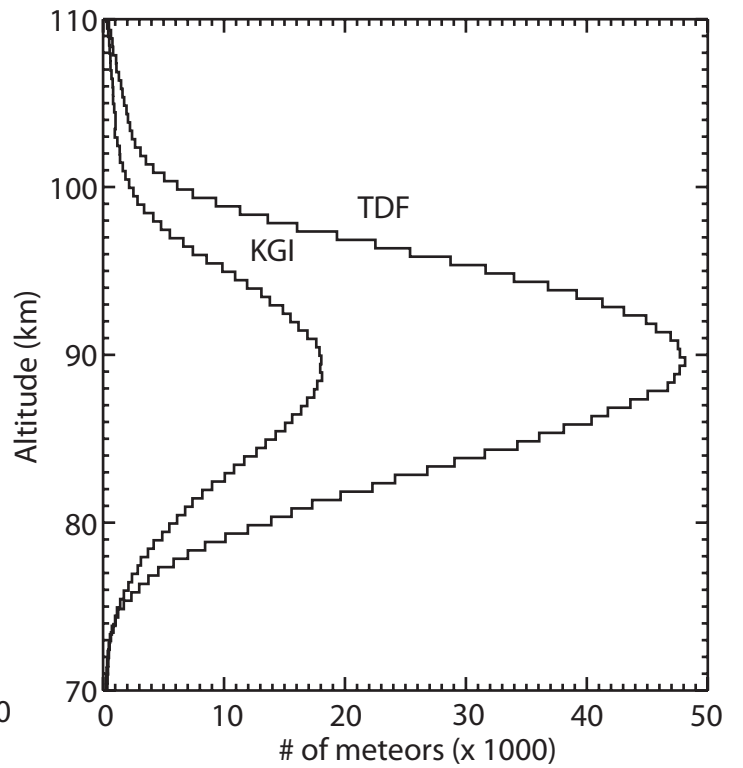
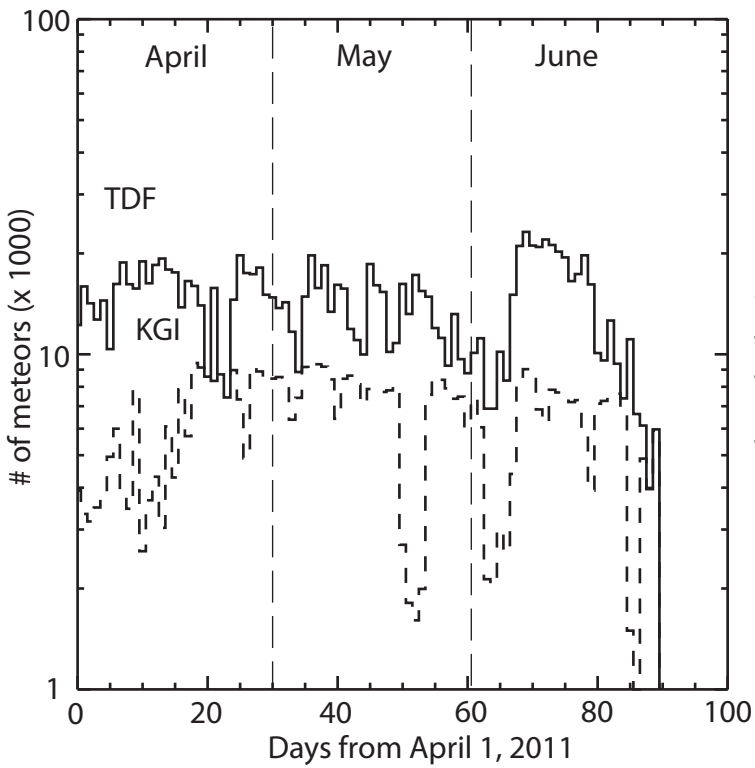
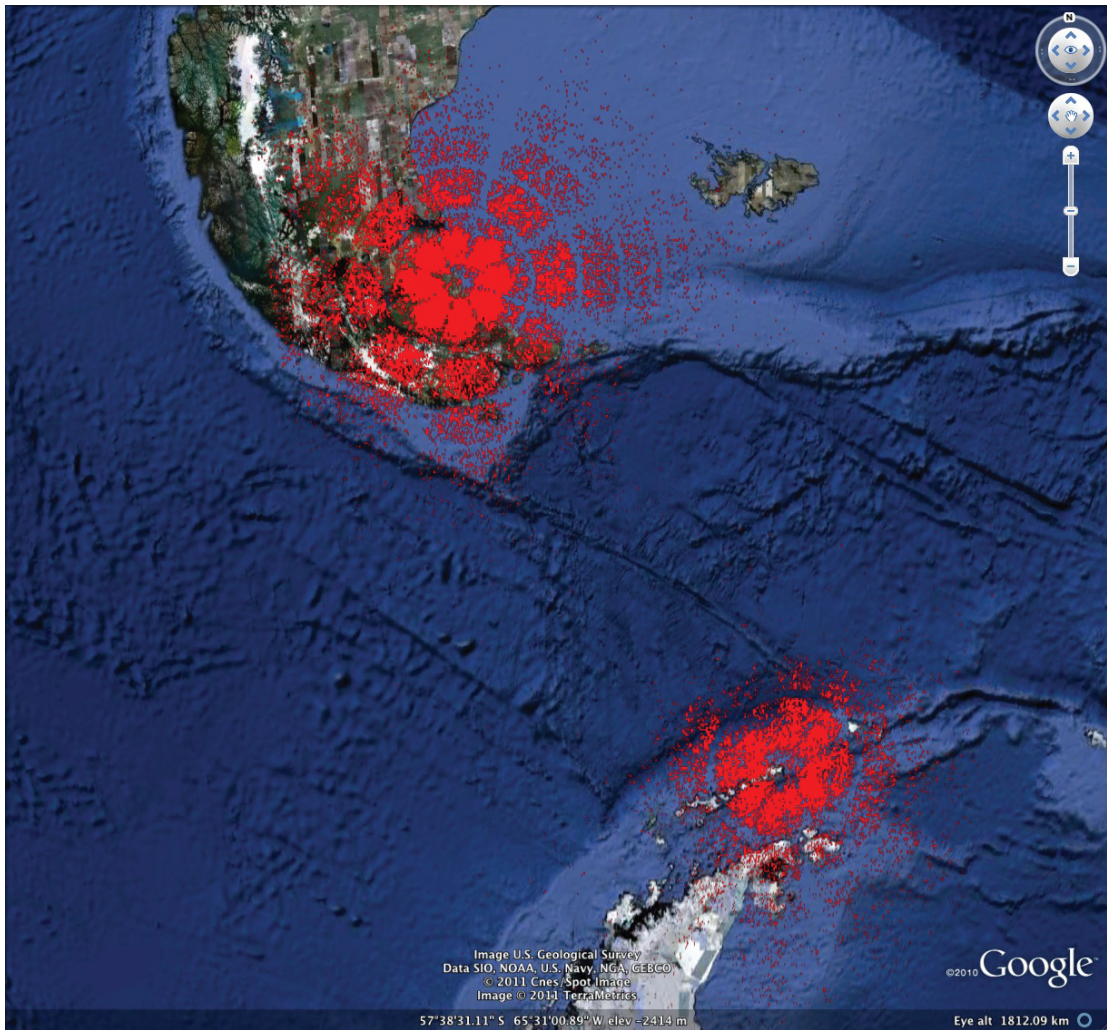
801 **Figure 10.** As in Figure 7, but for the semidiurnal tide.

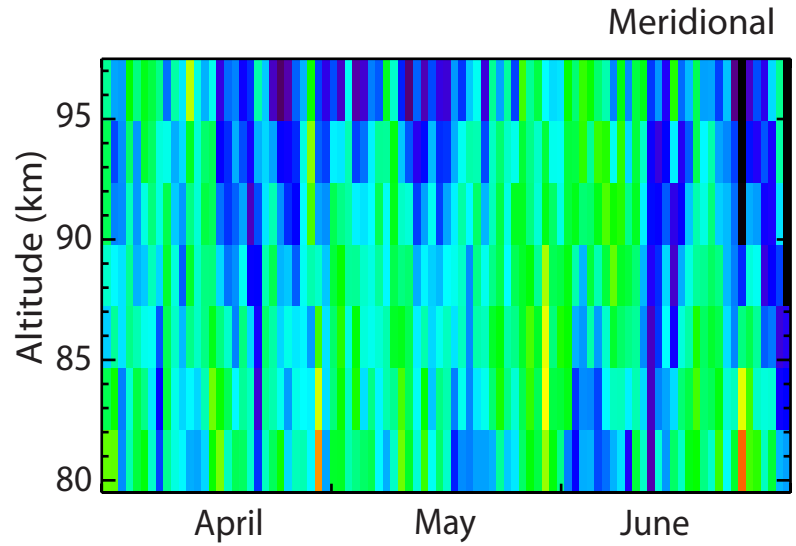
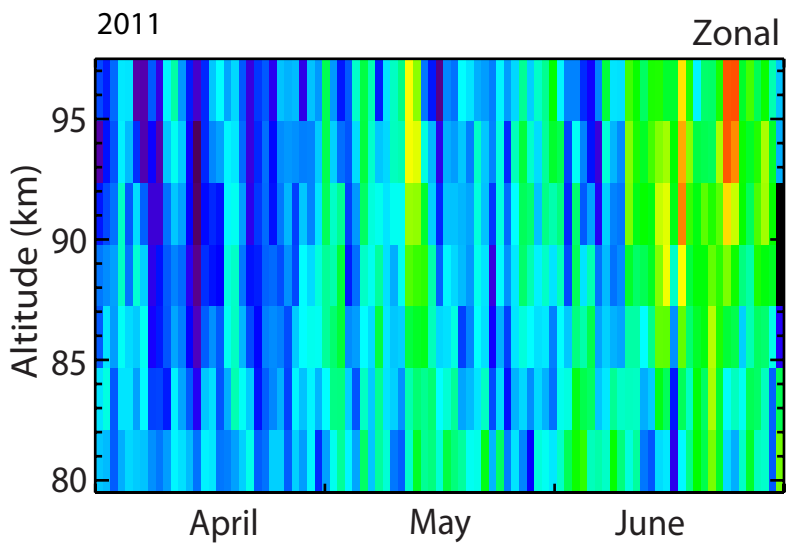
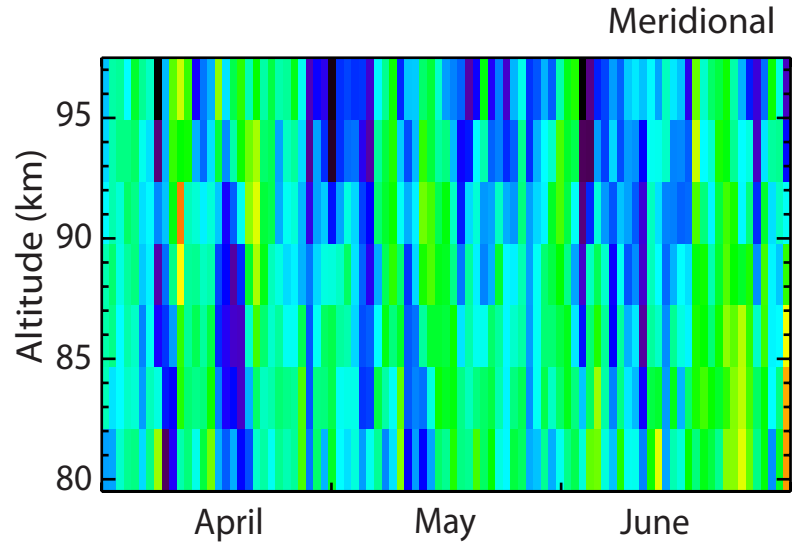
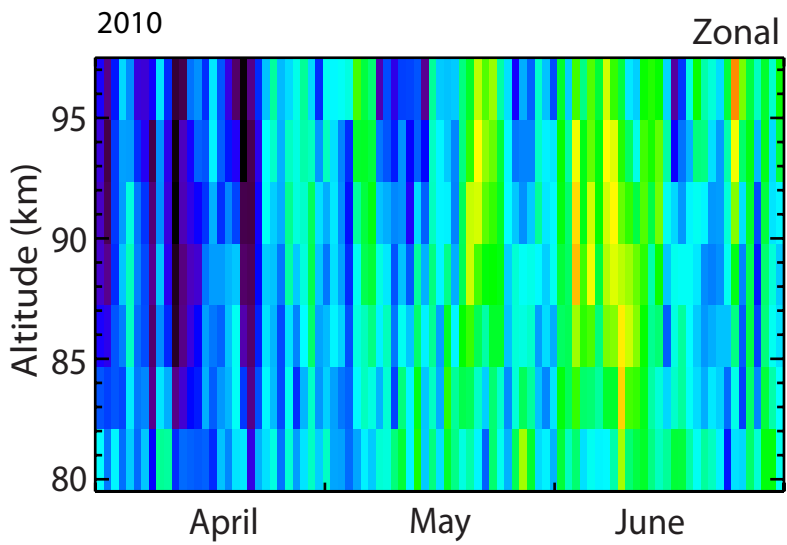
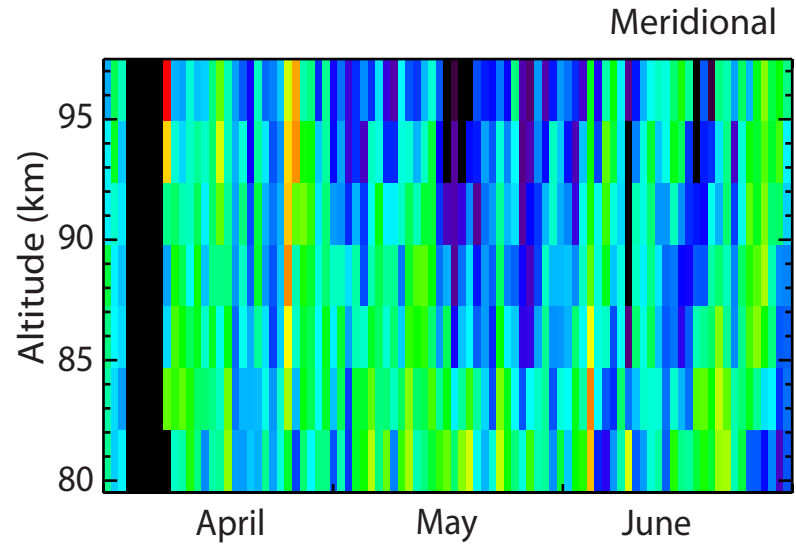
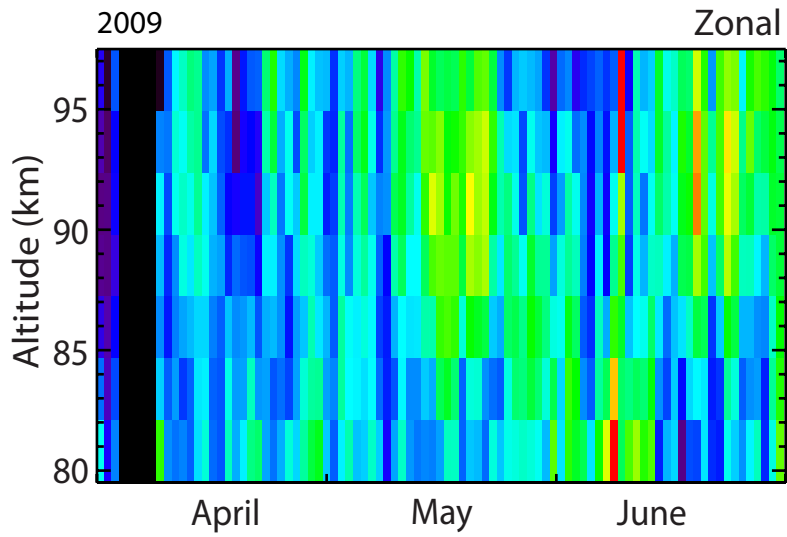
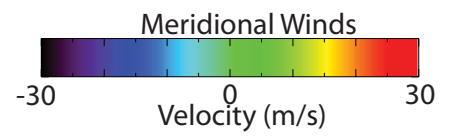
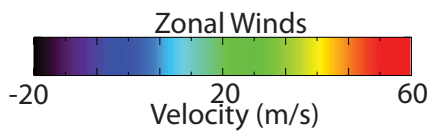
802 **Figure 11.** Monthly-mean (left) zonal and (right) meridional GW momentum fluxes for (top)

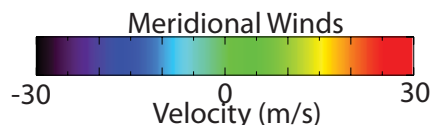
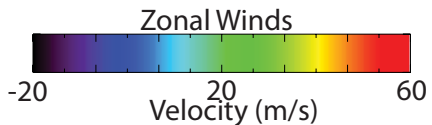
803 April, (middle) May, and (bottom) June of (solid lines) 2010 and (dashed lines) 2011 over (red)

804 DrAAMER and (blue) SAAMER.

805

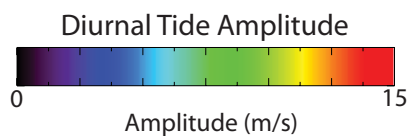
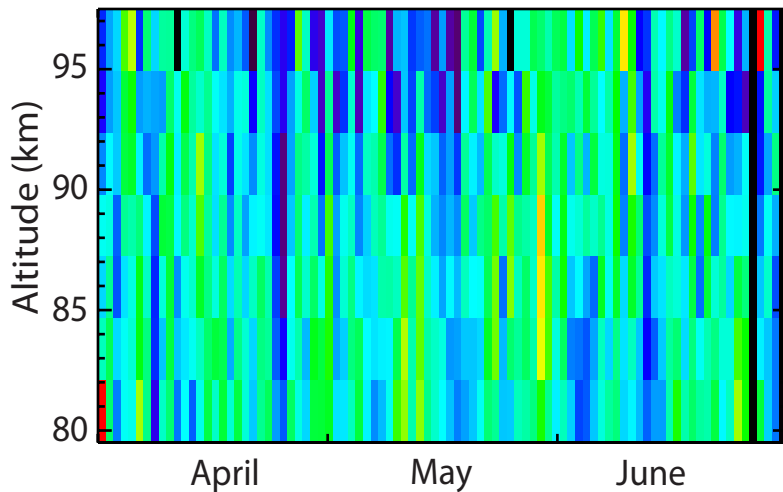
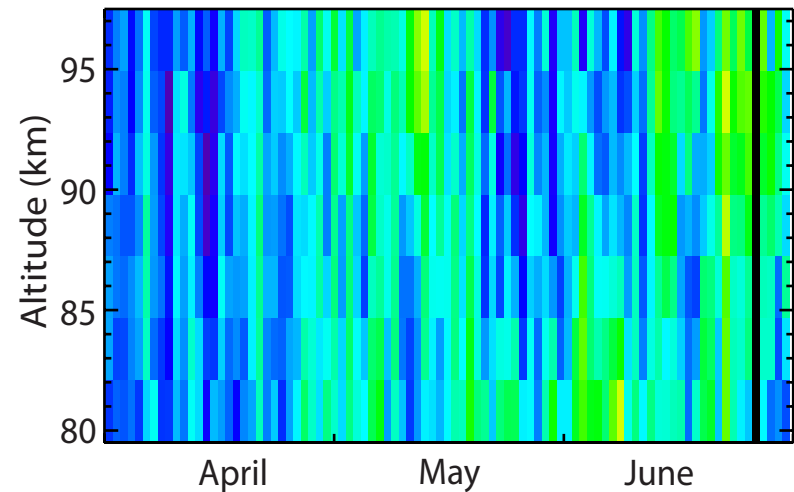






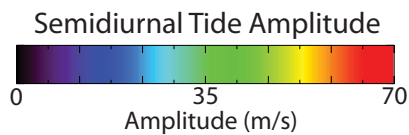
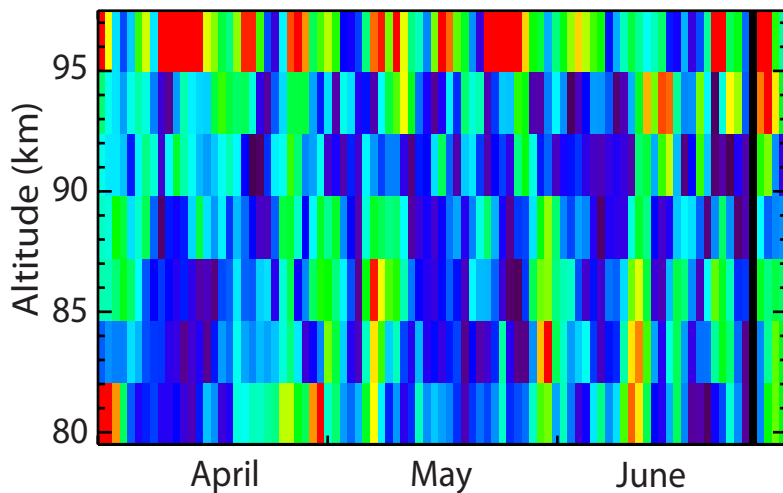
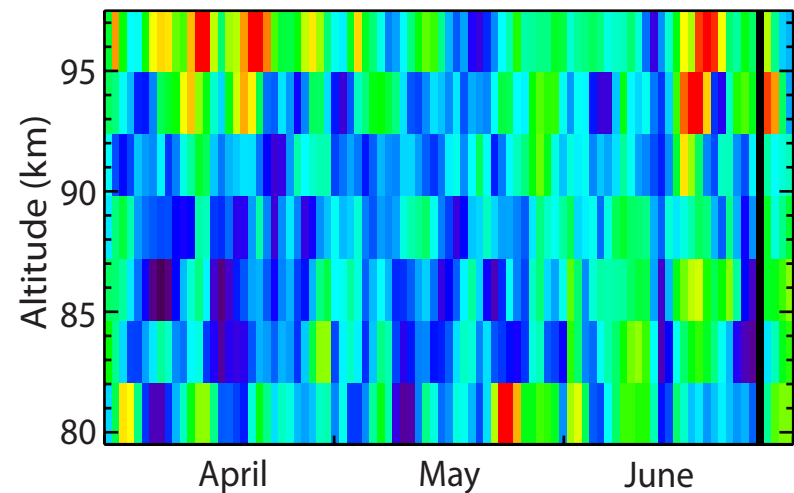
Zonal

Meridional



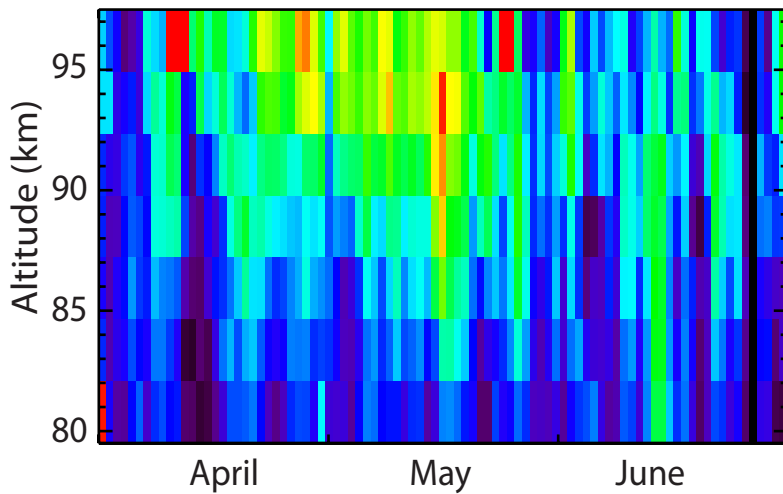
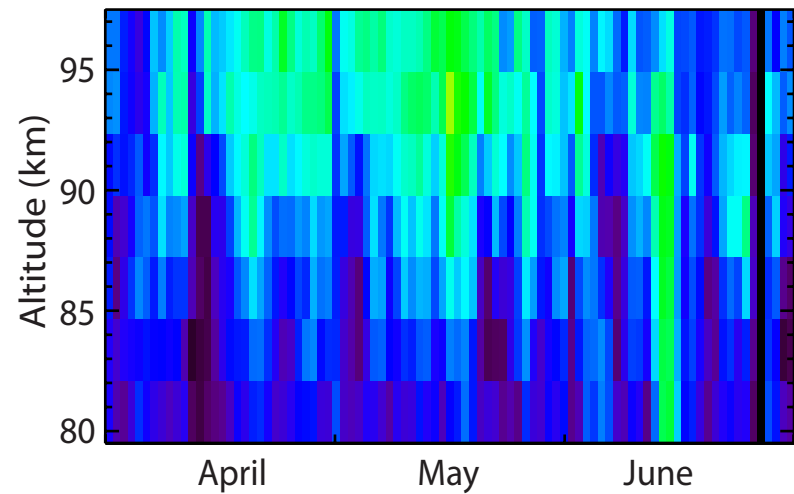
Zonal

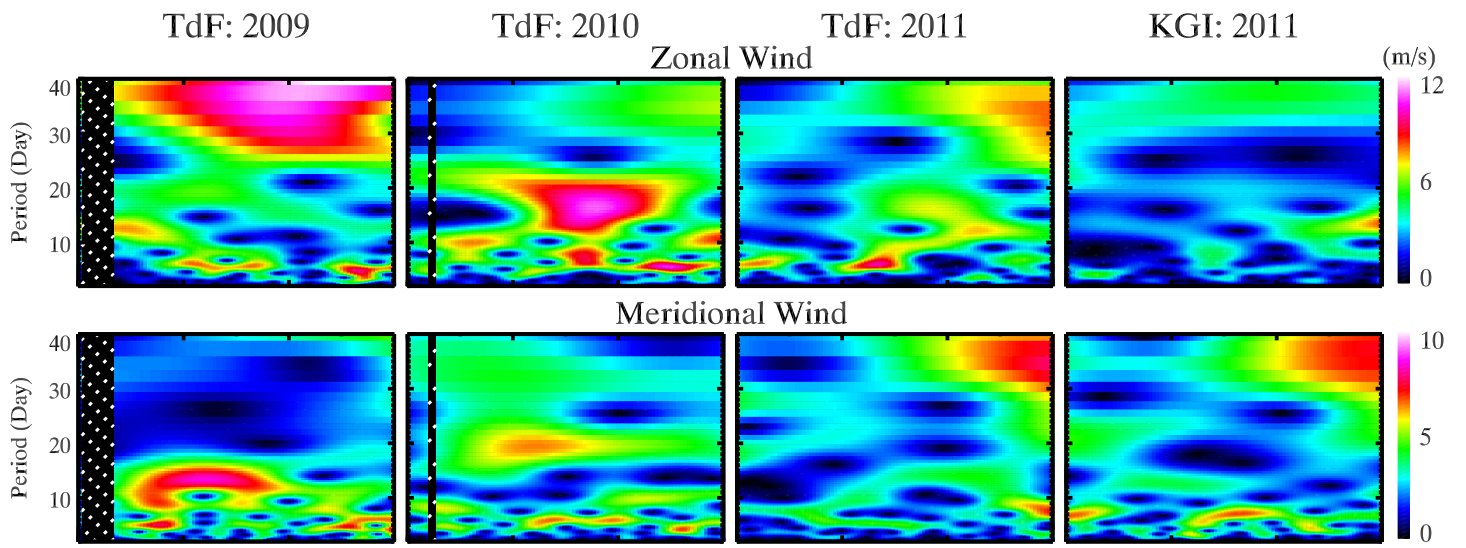
Meridional

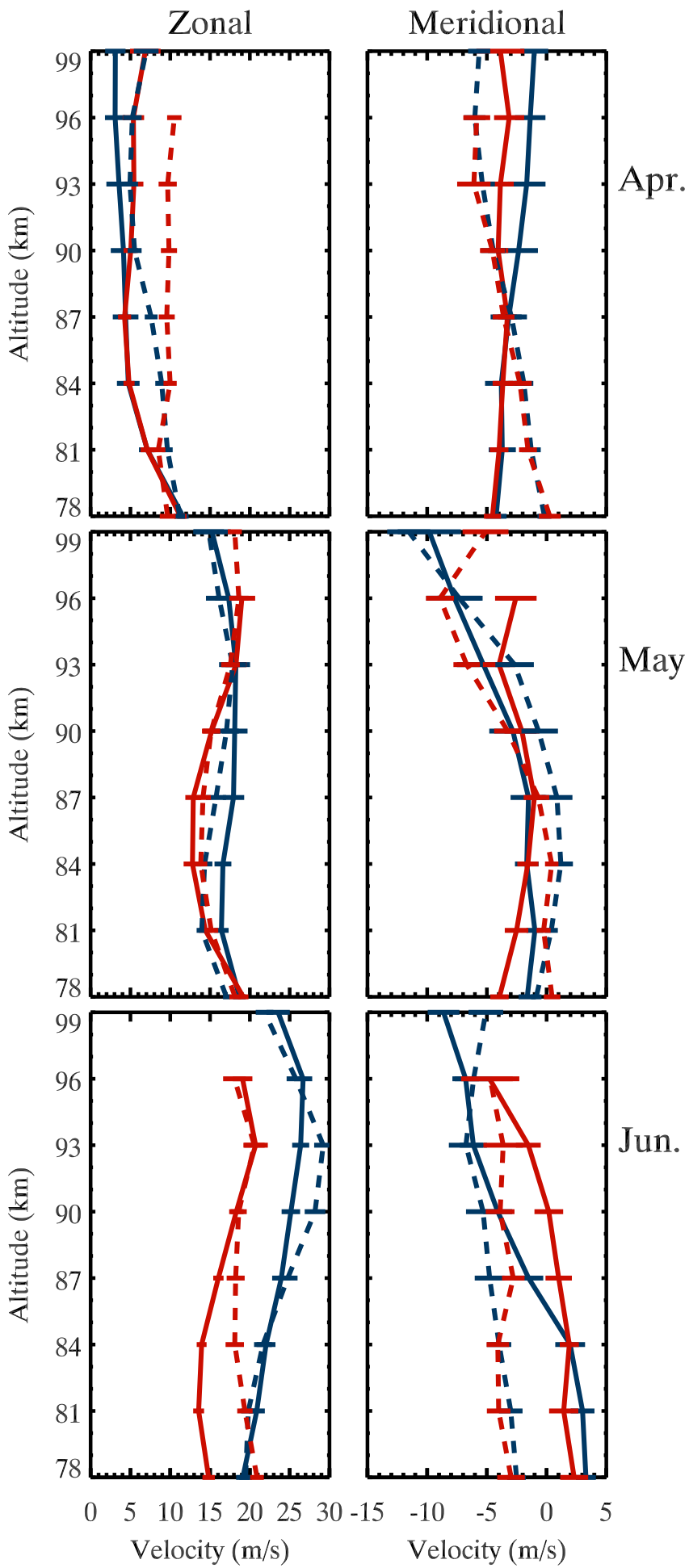


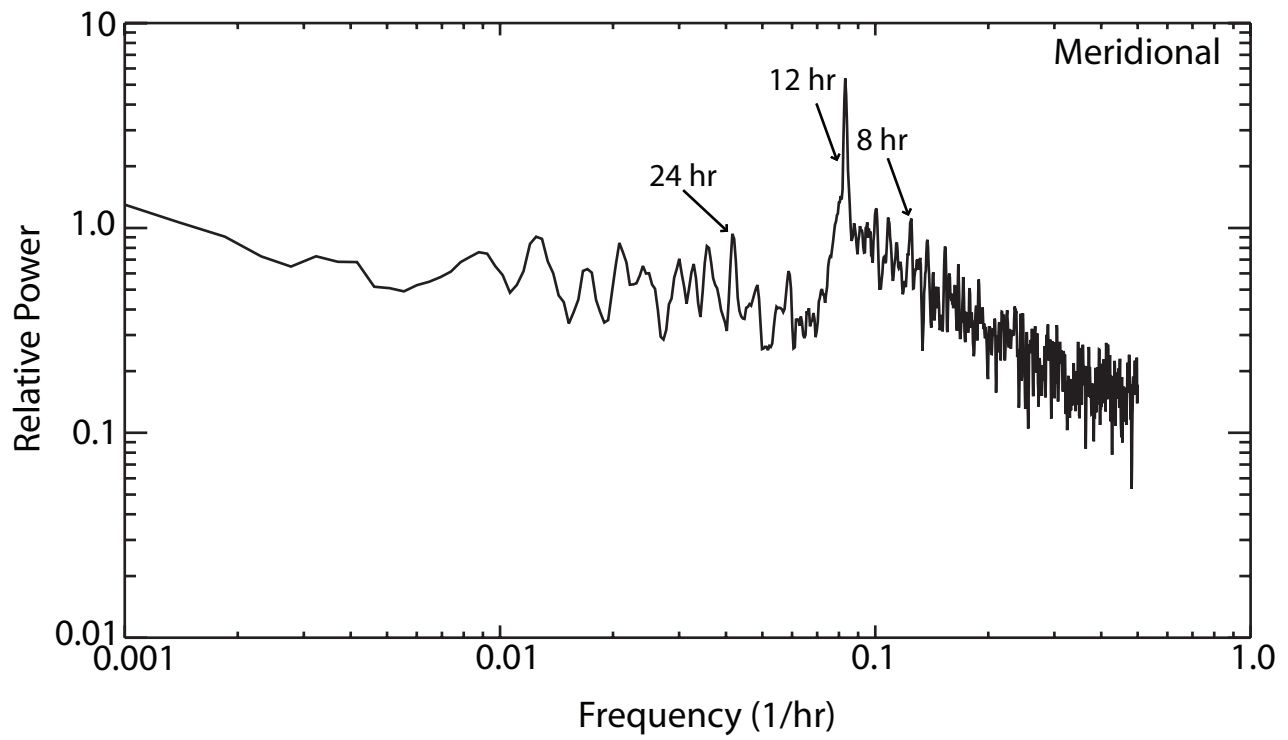
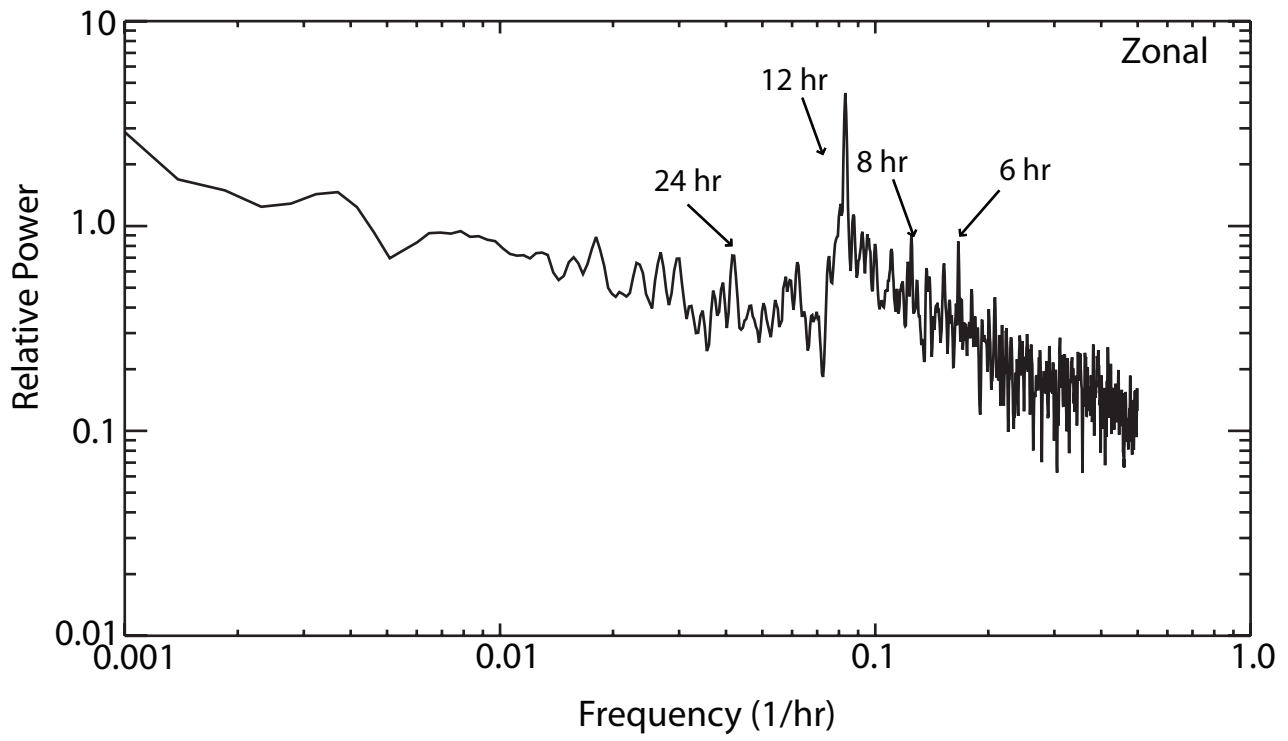
Zonal

Meridional

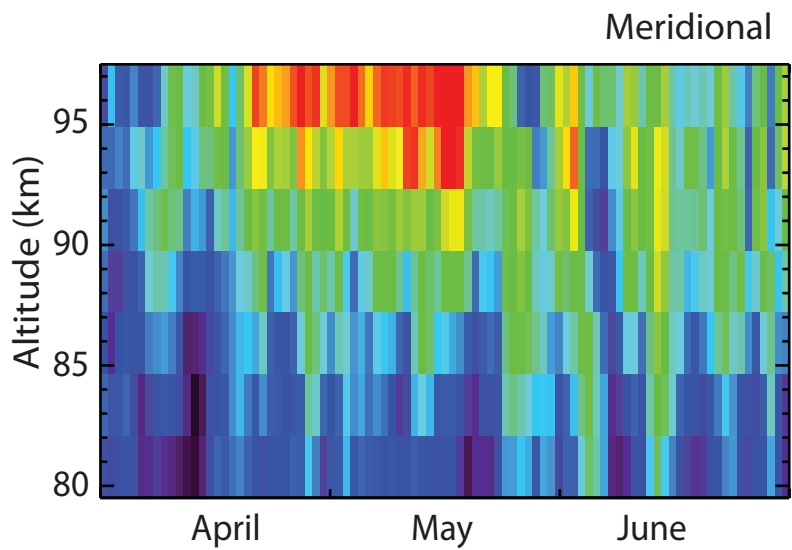
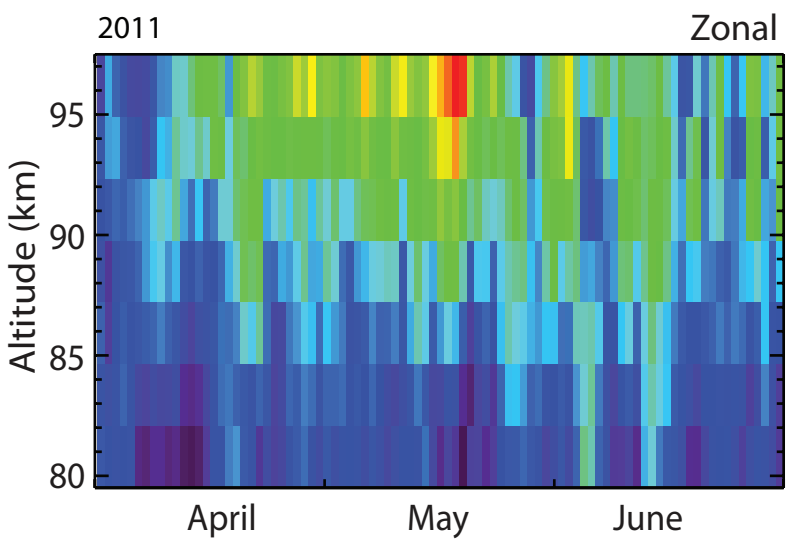
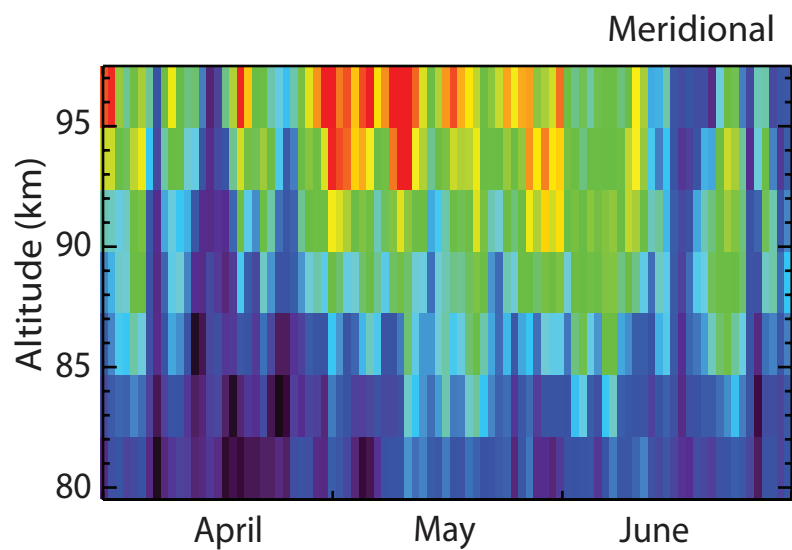
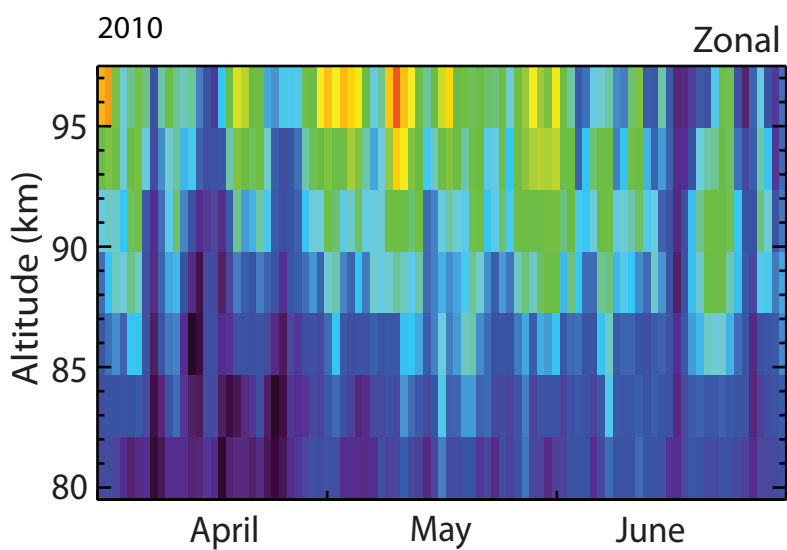
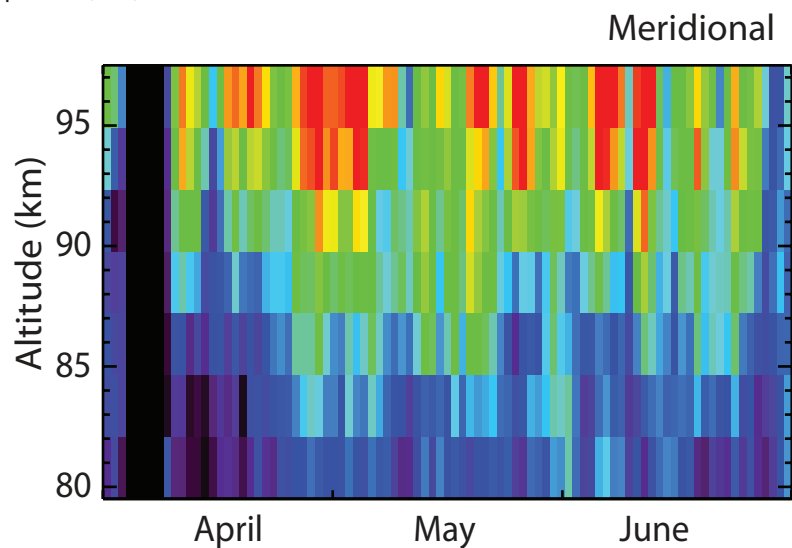
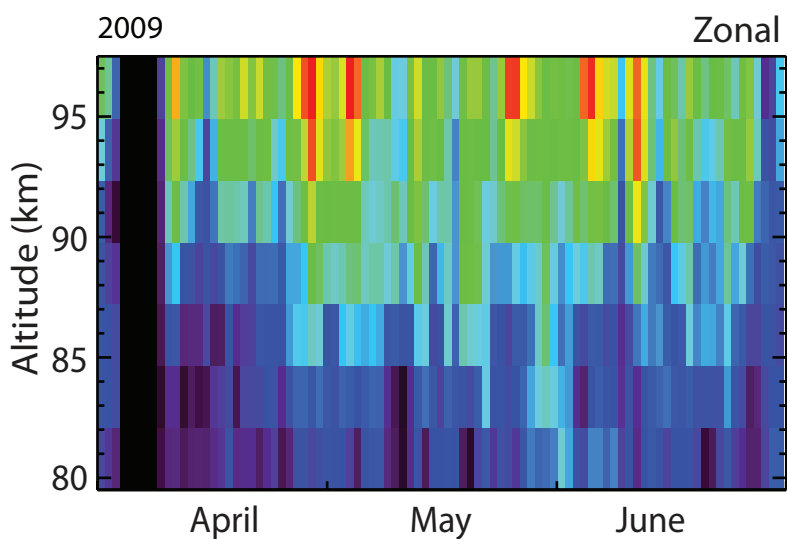
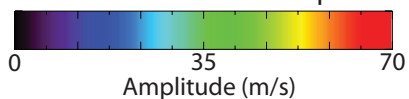








Semidiurnal Tide Amplitude

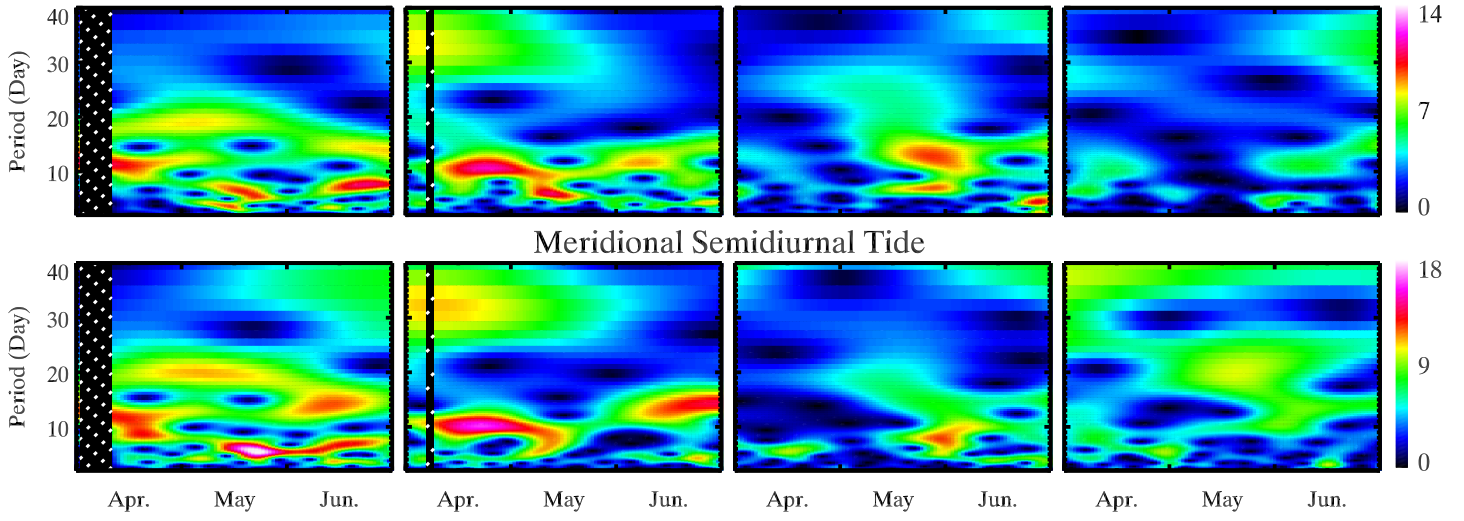


TdF: 2009

TdF: 2010
Zonal Semidiurnal Tide

TdF: 2011

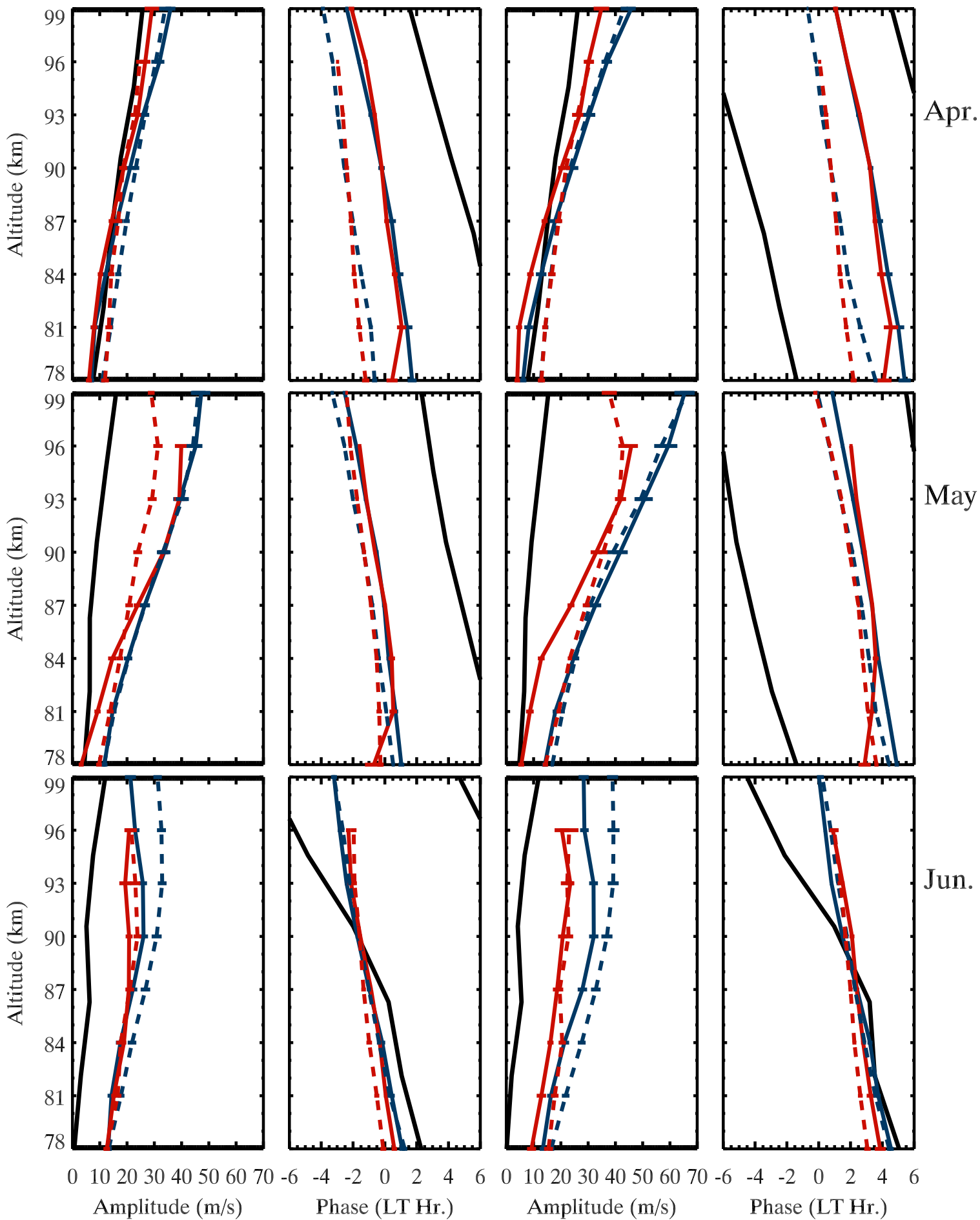
KGI: 2011



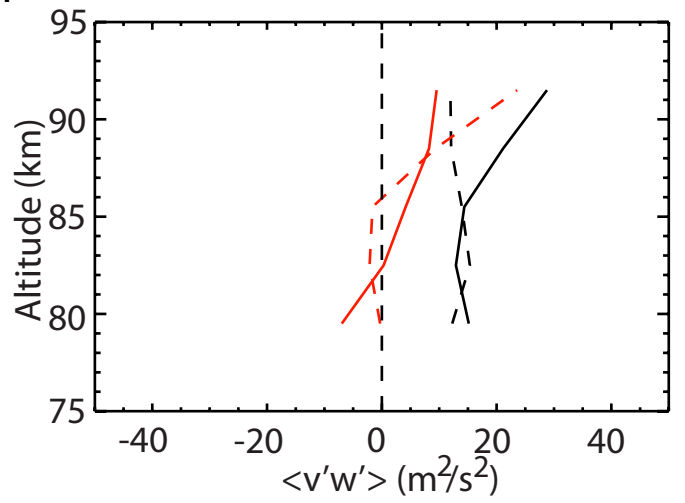
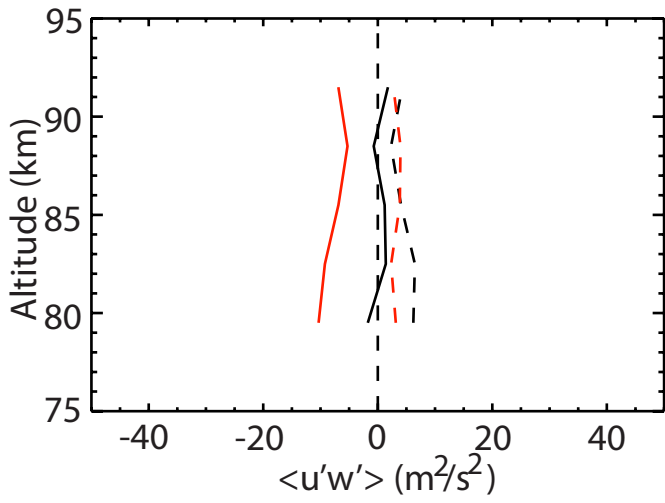
Semidiurnal Tide

Zonal

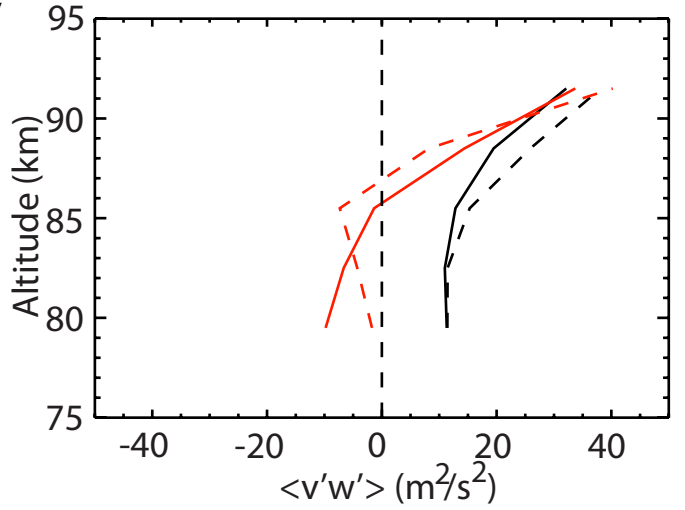
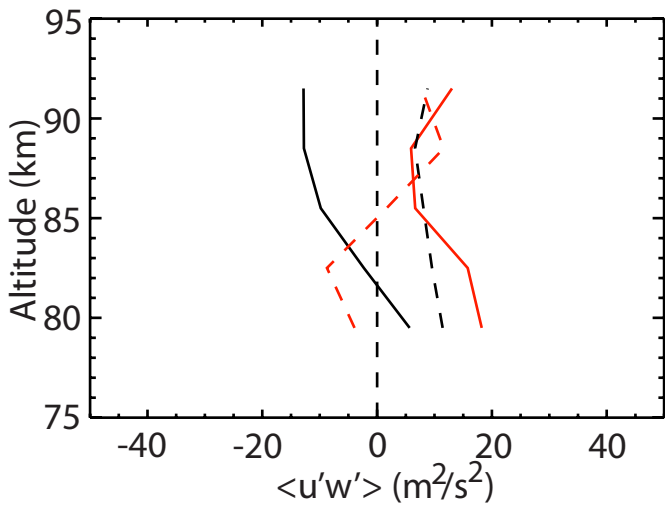
Meridional



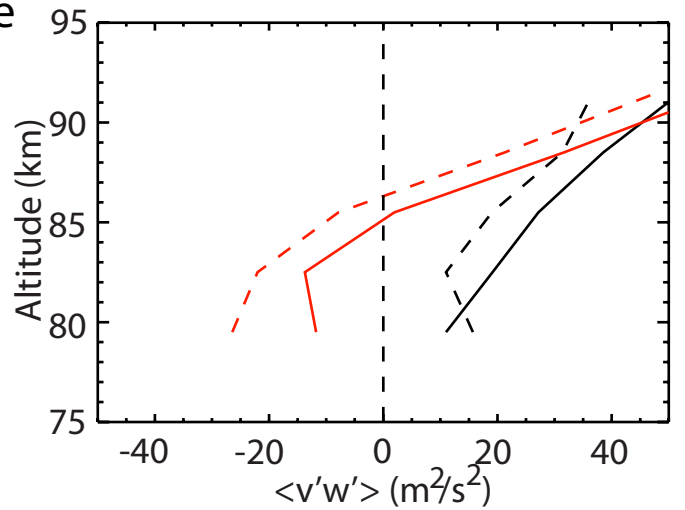
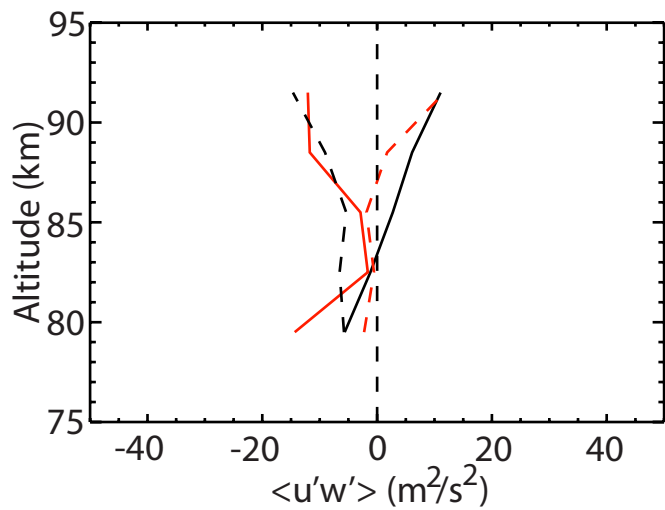
April



May



June



— 2010 — TDF
- - 2011 - - KGI